Technical Report 1608
September 1993

NOVAM Evaluation Utilizing Electro-Optics and Meteorological Data from KEY-90

S. G. Gathman, D. R. Jensen
NCCOSC, RDT&E Division

W. P. Hooper, J. E. James, H. E. Gerber
Naval Research Laboratory

K. Davidson
Naval Postgraduate School

M. H. Smith, I. E. Consterdine
University of Manchester Institute of Science and Technology, United Kingdom

G. de Leeuw, G. J. Kunz, M. M. Moerman
TNO Physics and Electronics Laboratory, The Netherlands

Technical Report 1608
September 1993

NOVAM Evaluation Utilizing Electro-Optics and Meteorological Data from KEY-90

S. G. Gathman, D. R. Jensen
NCCOSC, RDT&E Division

W. P. Hooper, J. E. James, H. E. Gerber
Naval Research Laboratory

K. Davidson
Naval Postgraduate School

M. H. Smith, I. E. Consterdine
University of Manchester Institute of Science and Technology, United Kingdom

G. de Leeuw, G. J. Kunz, M. M. Moerman
TNO Physics and Electronics Laboratory,
The Netherlands

NAVAL COMMAND, CONTROL AND OCEAN SURVEILLANCE CENTER
RDT&E DIVISION
San Diego, California 92152–5001

K. E. EVANS, CAPT, USN
Commanding Officer

R. T. SHEARER
Executive Director

ADMINISTRATIVE INFORMATION

The completion of this task represents the international cooperation of researchers from the United States, the United Kingdom, and the Netherlands. Funding for this project was supplied by the Naval Research Laboratory Detachment, Stennis Space Center, Mississippi under program element 0602435N, accession number DN302215.

Released by
R. A. Paulus, Head
Tropospheric Branch

Under authority of
J. H. Richter, Head
Ocean and Atmospheric
Sciences Division

ACKNOWLEDGEMENTS

The authors wish to acknowledge the efforts of certain people without whom this experiment could not have been carried out. First of all, the authors wish to thank Dr. Juergen Richter of NRaD, without whose support the project would not have been possible. Thanks are also due to Dr. Lothar Ruhnke of NRL for his support of the project. The authors want to thank Mr. Harry Tracy of Key Colony Beach, FL, the owner and captain of the *Renegade;* Gibb's flight service for operating the aircraft for the NOSC operations; and the NRL flight detachment for its part in the operation.

DM

CONTENTS

CONTENTS (continued)

FIGURES

CONTENTS (continued)

TABLES

CONTENTS (continued)

INTRODUCTION

To assess the performance of electro-optical (EO) device applications that involve vertical and slant paths through the marine atmosphere, we must know the vertical variation of the optical properties of this atmosphere. Two of the important properties are electromagnetic scattering and absorption at wavelengths from the visible to the far infrared (IR). Empirically derived expressions for the contributions of the aerosol exist for single levels; an example is the Navy Aerosol Mold (NAM) (Gathman, 1983a, 1983b, 1984) as found in LOWTRAN VI and VII (Kneizys et al., 1983). A physical model can extend the extinction prediction to higher altitudes.

A Naval Oceanic Vertical Aerosol Model (NOVAM) is being developed to provide the vertical variation of the optical/IR properties of the marine atmosphere (Gathman, 1989; de Leeuw et al., 1989a, 1989b; Davidson et al., 1990; Gathman et al., 1990). It uses meteorological profile information to account for the physical processes that influence the vertical aerosol structure. NOVAM, which is a mixture of empirical and dynamical models, describes the nonuniform as well as nonlogarithmic aerosol distributions that often exist in the marine atmospheric boundary layer (MABL). NOVAM itself uses NAM as a kernel and reverts to that model at the lowest altitudes of the marine boundary layer. NAM, which has been extensively updated, mathematically describes the aerosol size distribution at 10 m above the sea surface. The specific distribution depends on input data of wind speed (both current wind speed and the 24- hour average), visibility, and relative humidity. In both models, aerosol is produced by particles introduced into the marine atmosphere from white water phenomenon at the air–sea interface and from other sources such as gas-to-particle conversion or anthropologically and naturally generated continental aerosol.

The concentration of aerosol at any particular size interval depends on the source strengths of the aerosol production and the mixing process of scalar contaminants. On the other hand, the size of hygroscopic sea salt aerosol also depends on the relative humidity of the air parcel in which it finds itself immersed. As a hygroscopic aerosol picks up water vapor from the atmosphere and grows in size, it changes its chemical composition and thus its index of refraction. The NAM-generated aerosol at the surface is mixed throughout MABL by turbulent-controlled processes and is further modified by humidity effects. The MABL vertical structure determines the physics describing these processes. Various models describing the atmospheric vertical structures, such as a simple mixed-layer model (Fairall and Davidson, 1986) and a shallow convection case (Davidson and Fairall, 1986), are included in NOVAM. Provision has been made to include other models, such as models for deep convection, in the future. The selection of the model is based on the input parameters describing the vertical stratification (thermal stability, the presence of an inversion, and the inversion height), cloud cover, cloud type, wind speed, and the requested wavelength for the extinction calculation.

Gathman (1989) and de Leeuw et al. (1989a, 1989b) have presented an extensive description of NOVAM. NOVAM will perform best when all required input parameters are available. Thus, the input files need to contain information on the meteorological variables near the sea surface and the MABL vertical structure. Either a standard radiosonde observation or an instrumented aircraft making ascents or descents provides this information. A default relative humidity profile (Gathman, 1978) that is based on the surface observations is generated if the information on the vertical structure is not available.

NOVAM predicts the extinction and absorption of electro-optical energy as a function of altitude for a large number of wavelengths from the visible to the far IR. In the models, these properties are due to atmospheric aerosols only and molecular processes are not included. Relative humidity affects the size distribution of aerosol at any particular height. The model requires a certain amount of meteorological data for input. The availability of all input data adds to the accuracy of the model's

prediction. The types of inputs for the model involve the meteorological measurements that are commonly available. The model translates these inputs into predictions of mixing, source strengths, etc.

Data collected over the world's oceans are the original basis of NAM (Gathman, 1983a). Several users have since evaluated NAM (Gathman, 1989; Hughes, 1987) and used new experimental evidence to provide the basis of NAM's recent updating. NOVAM's development, however, is based on a more limited set of data collected over the eastern Pacific Ocean near the California coast. One method of testing NOVAM provides a simultaneous set of measurements of both the inputs to the model and the products of the model. The measurements and the predictions of the model would be identical, of course, in a perfect world. However, in real life, this does not usually happen. In reality, it is difficult to accurately estimate the measured extinction profile.

A preliminary NOVAM-estimated profile comparison (with one set of experimental data) that was also performed near the California coast yielded favorable results (de Leeuw et al., 1989b). A more comprehensive initial evaluation of NOVAM used an extended aerosol and extinction database obtained during the First International Satellite Cloud Climatology Program (ISCCP) Regional Experiment (FIRE) (Gerber et al., 1990; Gathman et al., 1990).

The FIRE experiment and the data sets used in the model development took place in the same Pacific coastal area. Therefore, the initial NOVAM evaluation from the FIRE data was basically a limited test for the performance of NOVAM. The model needs further evaluation in different geographical areas with different meteorological and oceanic conditions. Although several data sets that might be used to evaluate the model are available, they are not designed for this purpose and often one or more input parameters are missing. NOVAM performs best when all of these input parameters are available, and only in this case can the influence of missing inputs be tested. Therefore, the KEY-90 experiment was organized as the next step in the NOVAM validation process in a tropical trade wind situation where the physics differs strongly from those in the atmosphere near San Nicholas Island.

The general objective of the KEY-90 experiment was to provide an environment in which enough quality data could be obtained to verify the operation of NAM and NOVAM in a tropical ocean scenario. This was accomplished by simultaneously obtaining the meteorological parameters necessary to exercise NOVAM in its full capability and providing a "ground" truth measurement of the extinction profile at various wavelengths. The measured extinction profile provides a standard by which to judge the model extinction profile predictions.

OVERVIEW

AN OVERVIEW OF NOVAM/NAM EVALUATION TESTS

NOVAM requires two input files that contain information on the meteorological state of the atmosphere. The first describes the meteorological environment at the sea surface while the second describes the meteorological state of the column of air where the vertical structure of the optical/infrared parameters is desired. The second input file then produces a set of predicted optical/infrared properties for the same atmospheric column as an output. The evaluation and/or verification of this model requires a quality set of input meteorological data both at the surface and from a meteorological sounding. The results may then be judged by comparing the model output predictions to the independently measured properties of the atmospheric column.

The atmosphere is, however, a complex entity that contains many variations in space and time. These variations sometimes make it quite difficult to obtain an adequate measurement that really represents the desired quantity. In KEY-90, several measurements of the important data were obtained simultaneously by using several different instruments that operated independently. This redundancy was useful not only to ensure against instrument failure but to determine data quality. When several instruments gave readings that converged, we could be sure that differences in calibration and sampling were minimized. On the other hand, when a set of measurements indicated the data were consistently outside the envelope of acceptability, we could be sure that some sort of problem existed with this instrument, its calibration, or its sampling method. A considerable amount of effort went into the data evaluation used for the input "Surface Data File" of NOVAM. Various sorting techniques and statistical analysis of the data set produced the best possible numbers from the experiment. This "consensus" data and a short discussion of the data quality and what instruments were used in the averages appear in the data analysis section of this report.

A similar concern exists when we are providing data for the profile input. Here we have not only the meteorological quantities for a single level but also for a large number of levels. In addition, the structure of these meteorological profiles is important to the operation of NOVAM. The structure parameters are currently determined by an "expert" making a graphical analysis of the meteorological structure in the marine boundary layer. A semiautomatic method to determine these parameters is currently available in the personal computer version of NOVAM. The quality of the profile data, which we use to judge NOVAM's output at each level, is of greatest importance in the evaluation process. Of concern here is to what extent temporal and spatial variations and sampling techniques affect the optical/IR "standard" extinction profile by which the model results are to be judged.

Intercomparison of NOVAM calculations with direct measurements and calculations based on direct measurements determines the performance of the model and the accuracy of its predictions. Table 1 indicates the number of different types of intercomparisons available from the data collected in KEY-90. The physical and optical quantities listed in the left-hand column of table 1 show the quantities predicted by NOVAM as well as measured and/or calculated from the measurements. The table matrix element contains an "*" when the intercomparison between these two quantities is possible. The "surface dN/dr" is the aerosol size distribution that NOVAM estimates from the surface meteorology. These data should be the same as the measured aerosol size distributions obtained from the Particle Measurement Systems (PMS) aerosol spectrometer and the Rotorod system on the boat as well as the lowest altitude measurement made by the aircraft's PMS system. NOVAM and the aircraft PMS system can also determine the aerosol size distribution at various altitudes above the sea surface. Mie theory lets us convert an aerosol size distribution into extinction and backscatter coefficients as well as optical depths. Calculations made on measurements compare with NOVAM predictions and other methods of measuring these quantities.

Table 1. Comparisons possible between NOVAM predictions and KEY-90 measurements.

Comparison Tests	NOVAM	NOSC+	BOAT				NRL	TNO
		PMS	PMS roto-rod	HSS	P V M	sun photo-meter	aureole lidar	mini-lidar
Surface dN/dr	internal	*	*					
dN/dr at alt.	internal	*						
Surf. ext. @ .53 μ	*	* Mie	*Mie	*				
Ext. @ .53 μ at alt.	*	* Mie						
Surf. ext. @ 1.06 μ	*	* Mie	* Mie				*	*
Ext. @ 1.06 μ at alt.	*	* Mie					*	*
Surf. ext. @ 3.5 μ	*	* Mie	* Mie					
Ext. @ 3.5 μ at alt.	*	* Mie						
Surf. ext. @ 10.6 μ	*	* Mie	* Mie		*			
Ext. @ 10.6 μ at alt.	*	* Mie						
Optical depth @ .53 μ	* calc 1	* calc 2				*	*	
Surf. back-scatter @ 1.06 μ	* calc 1	* calc 2	* calc 2				*	*
Back-scatter at alt. @ 1.06 μ	* calc 1	* calc 2					*	*

+ The Naval Ocean Systems Center (NOSC) has been renamed the Naval Command, Control and Ocean Surveillance Center (NCCOSC) Research, Development, Test and Evaluation Division (RDT&E Division), also known as NRaD.

In table 1, there are 31 different intercomparisons between NOVAM predictions and measurements for the visible, near IR, 3- to 5- and 8- to 12-μm wavelengths. Of course, not all intercomparisons are available on all days of the experiment, e.g., the sun photometer measurement requires a

clear line of sight between the measurement site and the sun and is not possible on cloudy days. Comparisons between items in the table should take into account other factors. For instance, when several measurements are available for a particular test, we need to know how well the measurements agree with each other. When measurements disagree and there is no reason to believe one measurement over another, then it is reasonable to say that NOVAM was successful in its predictions if the predictions fall within the envelope of the "measurements."

PARTICIPANTS

The U.S. Navy, in conjunction with the Exploratory Development Program, "Atmospheric Effects of Electromagnetic/Electro-Optical (EM/EO) Propagation," sponsored the KEY-90 experiment. It was, however, an international effort involving close cooperation between institutes from the U.S.A, U.K., and the Netherlands (see table 2). The instrumentation contributed by each institute for the boat, the aircraft and the shore station are listed in later tables of this report.

Table 2. NOVAM evaluation: Participating institutions and principal investigators (PIs).

Institution	Country	P.I.
Naval Research Laboratory (NRL) *	US	S.G. Gathman
Naval Ocean Systems Center (NOSC)	US	D.R. Jensen
Naval Postgraduate School (NPS)	US	K.L. Davidson
University of Manchester, Institute of Science and Technology (UMIST)	UK	M.H. Smith
TNO Physics and Electronics Laboratory	NL	G. de Leeuw

* chief scientist

The Naval Air Station in Key West, FL, and instrumentation at the Marathon airport collected other meteorological data. A sister experiment called the Infrared Analysis Measurement and Modeling Program (IRAMMP) occurred at this time and place in the Keys . In a cooperative data exchange effort, Areté Associates, under contract to provide wave data for IRAMMP, also provided the KEY-90 database with wave data from two buoys located outside of the reef. The buoys were 7 km and 11 km out from the shore and were in place from 6 to 19 July. These buoys provided information on the root mean square (rms) wave heights and the power spectra of the waves. In addition to the data collected with this instrumentation, visual and manual weather observations were made from time to time by various participants.

EXPERIMENTS AND RESPONSIBILITIES OF EACH PARTICIPANT

Naval Research Laboratory (NRL): Surface Measurements

NRL was responsible for outfitting the fishing boat *Renegade* for the experiment. NRL installed a large structure on the bow deck of the boat; personnel could mount the various instruments on this large structure. In addition to the usual meteorological instrumentation such as heading, wind, sea surface temperature, air temperature, and relative humidity, NRL supplied instruments to measure the "visibility" directly by using the *HSS* visiometer and an independent measurement of infrared

extinction that uses the particle volume meter (PVM) on loan from Gerber Scientific, Inc. An additional determination of the extinction made by this device increased the amount of data to compare with the calculations made from the aerosol size distribution measurements obtained from the PMS devices on the boat and the aircraft. An additional check on the overall accuracy of the optical measurements from the aircraft and the model predictions came from a simple device known as the sun photometer. This device measures the optical depth of the atmosphere from the earth surface to the sun. A manual radon counter was also on board to provide measurements of radon 222. These measurements will be used in the estimates of the air mass parameter for the modeling tests. On loan to NOSC and NRL was an *Environment One* condensation nuclei, (CN) counter that was used to investigate the relationship between the NAM/NOVAM total small aerosol concentration, the atmospheric radon concentration, and the CN count.

Naval Ocean Systems Center (NOSC): Airborne Platform and Surface Measurements

The NOSC instrumented aircraft (Jensen, 1978) was the key tool in providing the profile information on both the meteorological and aerosol structure of the marine atmosphere throughout the KEY-90 experiment. In this function, it was the principal device to determine—*in situ*—the profile of the aerosol size distribution in the air column above the boat, as well as to obtain simultaneous temperature and relative humidity profiles for each test. Optical and IR extinction were calculated from the aerosol data by means of the Mie scattering theory. The aircraft was the essential element in the evaluation of NOVAM for the KEY-90 experiment. In addition, this versatile airborne laboratory was able to map out sea surface temperatures and provide other meteorological data for the sister experiment (IRAMMP horizon measurement test) taking place concurrently with the KEY-90 experiment. NOSC also provided instrumentation located on shore for the evaluation of the air mass parameter and the average winds used in NOVAM.

Naval Research Laboratory (NRL): Airborne Lidar

The KEY-90 experiment provides an opportunity to compare EO quantities calculated from the airborne aureole measurements with other independent *in situ* measurements and to use lidar-derived data for NOVAM evaluation. Hooper and Gerber (1986, 1988), using theoretical models, computer simulations, and ground-base measurements, studied the aureole concept and its application in remote sensing of the atmosphere. The aureole lidar requires the sea surface to reflect the beam and, hence, the technique requires that the lidar be supported by an elevated platform, such as an aircraft, and pointed straight downward. The data collected during the KEY-90 experiment provided an important "first field test" of the technique. The comparison of lidar data with almost simultaneous *in situ* aerosol measurements from the NOSC aircraft yielded an independent verification of the techniques. The airborne lidar produced a large-scale map of aerosol variations that is useful in interpreting *in situ* measurements from the boat and aircraft. Individual lidar profiles had an altitude resolution of 7.5 m. Collectively, the lidar profiles revealed the large-scale variation of aerosol scattering in the atmospheric cross section defined by the flight path (approximately 65 km). This variation of aerosol scattering ranged in height from the surface to the aircraft altitude (typically 3 km). Within this cross section, the boundary-layer depth, individual cell size, and cloud height are identifiable.

Naval Postgraduate School (NPS): NOVAM-Related Analysis

NPS collected additional data to be used in the NOVAM performance evaluation for convective boundary-layer structure cases. NPS provided a self-contained Weather Pak system that supplied much of the standard meteorological data obtained on the boat as well as the equipment to make standard radiosonde profiles. Radiosondes will be the normal mode of input to NOVAM, because

soundings from specially instrumented aircraft are not usually available. From 9 July 1990 through 19 July 1990, 18 radiosonde launches were made from the boat. Sixteen of these 18 launches provided useful data. Three of these launches were made at the pier. The profile parameters deduced from the radiosondes and the NOSC aircraft spirals provided essential input to NOVAM. The radiosondes and the nearly simultaneous aircraft meteorological profiles provided intercorroboration on the accuracy and variability of the meteorological profiles and the structure factors derived from the meteorological profiles for use in exercising NOVAM.

University of Manchester, Institute of Science and Technology (UMIST): Aerosol Size Distributions

The main purpose for the participation of UMIST in the KEY-90 measurement program was to provide aerosol particle concentration observations onboard the instrumented small boat. A PMS FSSP-100 optical particle counter located on the instrument tower that had been mounted upon the bow of the boat made these measurements. For the KEY-90 project, a basic aerosol sampling period of 10 seconds was selected to provide appropriate temporal resolution, though generally stored spectra have subsequently been integrated over longer periods in order to improve the sampling statistics.

Compared with most other UMIST marine aerosol investigations, winds during KEY-90 were generally much lighter and the preliminary analysis of these data suggests that the prevailing wind speed was much less dominant in determining the aerosol loading. High air and sea temperatures, which consequently have high water vapor concentrations and relative humidities, probably modified the aerosol particle spectra. Moreover, frequent thunderstorms and large convective cells obviously played a significant role in removing particulates from the atmosphere and thus modifying the observed spectra.

University of Manchester, Institute of Science and Technology (UMIST): Moisture and Momentum Fluxes

An additional package of instruments was installed on the boat. The purpose of this package of instruments was to provide high-frequency measurements of vector wind speed and water vapor density, so wind stress and water vapor fluxes could be determined by means of the "dissipation" technique. The values of u_* obtained during the observational periods are available to assist with the interpretation of the aerosol measurements.

TNO – Physics and Electronics Laboratory (FEL): Aerosol and Lidar Measurements

The TNO Physics and Electronics Laboratory participated in the KEY-90 experiment by providing aerosol and lidar measurements. The large aerosols close to the water surface were measured by means of a system of Rotorods mounted on a buoy and launched from the boat. In addition, a slant path lidar mapped the structure of atmospheric backscatter and extinction coefficients throughout the marine boundary in the vicinity of Bonefish Towers (a Marathon high-rise building) before, during, and after each experiment. In addition to providing information in the evaluation process of NOVAM, these measurements provided independent information on the source function for marine aerosol and the structure of aerosol properties above a tropical ocean area. These data can be used for the evaluation and improvement of surface models such as NAM.

The Rotorod device extended the range of the size distributions of the PMS system on the boat. The concentrations of these large particles are most important for the extinction properties in the far infrared. A comparison of NAM with the HEXMAX data set has shown a discrepancy at high winds

(G. de Leeuw, to be published). A reliable description of the influence of these large particles may require the addition of a fourth mode to NAM (de Leeuw et al., 1989a, 1989).

The third objective of the TNO Physics and Electronics Laboratory was to evaluate NOVAM by using extinction and backscatter profiles measured with lidar. Lidar is a unique tool for remote sensing of atmospheric optical parameters. In this way, it can often see atmospheric, boundary-layer dynamical processes in action. Direct measurement of these processes usually requires airborne platforms that are expensive to operate, but have the advantage of being able to cover large areas in a limited time. The TNO – FEL lidar operated semicontinuously from a fixed point and yielded a time series of boundary-layer profiles that showed its evolution over the range of the lidar. Lidar systems installed in airborne platforms, which have the same disadvantages as other airborne measurements (high cost and limited operation time), measured the spatial variability of the boundary-layer vertical structure.

OPERATIONAL PROCEDURES

The KEY-90 experiment took place near the Florida Keys in the Straits of Florida in the area southeast of Marathon, FL, from 2 to 19 July 1990. Figure 1 is a map of the region around the KEY-90 experiment area and it shows the location of the experiment site with respect to other geographical areas. This location and our ability to make boat and aircraft measurements placed the experiment in a "tropical" trade wind regime at a minimum of cost and let the experiment be away from land influences and the aerosol data be away from major continental effects.

The base of operations for the experiments was Marathon, FL (about 81.06° W; 24.40° N). A small boat, the *Renegade*, was the platform for surface measurements of aerosols and meteorological parameters as well as for radiosonde launches. Personnel from UMIST, NRL, NPS, and TNO – FEL made the measurements aboard the boat. Other instruments located ashore in Marathon collected surface data. The NOSC aircraft used the local airport in Marathon for its base of operation, while the NRL P3 aircraft was based out of the Key West Naval Air Station. Both the NOSC and the NRL aircraft and the TNO – FEL ground-based lidar collected data on the vertical structure of extinction and backscatter. The NOSC aircraft and the NPS radiosondes measured temperature and humidity profiles that were required as input to the NOVAM program. The wave measurements were made in a more or less continuous operating mode by two special buoys anchored off shore. The buoys sent the data to a shore station via a radio link.

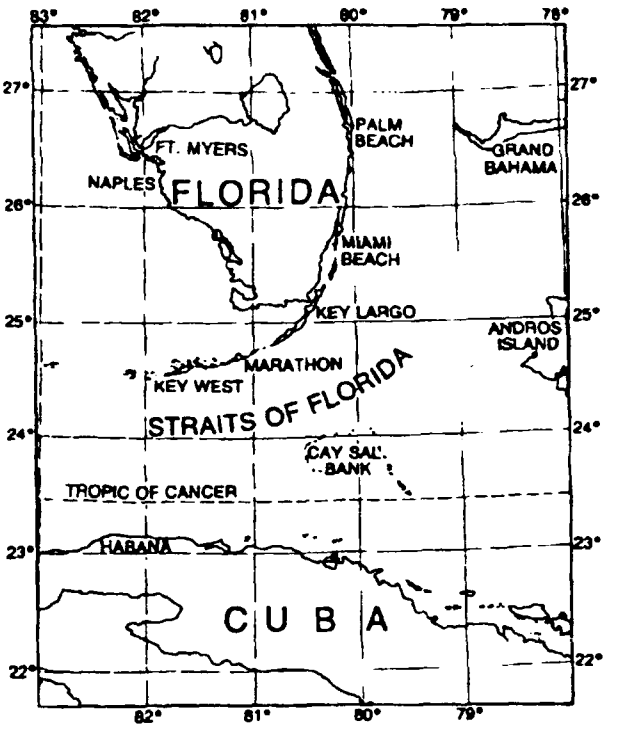

Figure 1. Map of the Straits of Florida where the KEY-90 experiment took place in July 1990.

A planning and coordination session preceded each experiment. At this session, the plans for the particular experiment and the timing and clearance questions were discussed. Although each of the various parties coordinating the measurements could communicate with each other via radio, such communication was not always reliable and prearranged schedules were necessary to successfully concluded the experiment. The type of data collected and the first impressions from the previous day were discussed in these information exchanges. First-cut graphs of the important parameters provided insight into the physics of the situation and helped make improvements in the experimental procedure on the following day. Copies of data logs and floppy disks with appropriate data were exchanged as far as they were available.

The measurements were made during different periods throughout the 24-hour day. This prevented the observations from being masked by diurnal effects. The limiting time for the experiment was the amount of time each day the *Renegade* took to get from the shore base to the rendezvous point and to return.

Manual and automatic measurements were made continuously from the time the boat left the harbor until it returned. The instruments aboard the boat were checked and calibrated while sailing to the rendezvous point. The boat stopped upon arrival at the rendezvous point and the TNO Rotorod buoy was put over the starboard side of the boat while a radiosonde was launched. The Rotorod device is described in detail in chapter 4 of a TNO report (de Leeuw et al., 1991). Usually, two Rotorod profiles were measured at each location. Between these two profile measurements, the boat moved upwind only fast enough to keep steerage so that the UMIST aerosol measurements with the PMS optical particle counters were pointing into the wind. At the same time, some Rotorod measurements were made beside the PMS equipment for comparison purposes and for NAM validation. While the boat was in this vicinity, an aircraft profile was always taken nearby with the NOSC aircraft. All flights were coordinated with the ground and surface-based experimental platforms.

Before each flight, the NRL aircraft laser and telescope were aligned. The detectors and amplifiers were calibrated by using a ground target. A neutral density filter inserted into the path of this ground setup provided a reduced signal for the calibration. During the flights, a series of race track circuits was flown over the boat. The northern turn took place southwest of the Florida Keys. The southern turn took place north of the Cay Sal Bank Islands. Each leg was approximately 65 km long and the entire circuit took approximately 20 minutes. The initial data were taken at a 3-km altitude. However, to test the equipment, measurements from altitudes of 5 and 6 km were also made. After each flight day, the sensitivity of the reflection to aircraft attitude was tested with a series of turns (left to right and 5° or 10°), climbs, and ascents.

Coordinated measurements were made between the boat and the aircraft to allow for simultaneous measurements of surface data and profiles. In this way, the profiling capability of the NOSC airborne platform provided the needed input data with which to test NOVAM. In addition, the aircraft studied horizontal variability on their way to the meeting point. The approximate coordinates of these rendezvous points are given in table 3. In case of showers, positions were chosen outside the precipitation area.

Table 3. Rendezvous positions.

Longitude	Latitude
80.55° W	24.35° N
80.55° W	24.22° N
80.45° W	24.22° N
80.52° W	24.32° N
80.40° W	24.35° N

In summary, the daily operation periods consisted of the following:

- Measurements were made from the chartered vessel *Renegade* in its operations east of Marathon.
- The lidar aboard the NRL P3 mapped the backscatter coefficients for a given radial in the vicinity of the *Renegade*.
- From its vantage point in a local high-rise building known as Bonefish Towers, TNO obtained vertical profiles of lidar backscatter in the vicinity east of Marathon.
- The NOSC airborne platform made vertical spirals near the *Renegade* as well as constant altitude runs.
- The wave buoys located offshore and the wind and radon measurement system located on the island made continuous observations.

INSTRUMENTATION

INSTRUMENTATION ABOARD THE RENEGADE

Onboard the *Renegade*, a 2-m tower was constructed and fastened to the bow of the boat. This tower was a place to mount most of the sensors used on the boat. Power from the boat's generators activated the instrument electronics and computers that were situated in the forward cabin. Table 4 lists the instruments contributed by the various experimenters and institutions. The table mentions several times that the "mini weather station" provided by NPS gave certain key information. This device is known as a "weather pak" manufactured by Coastal Climate Corporation. In addition, NRL installed a bivane anemometer and compass that recorded boat motion and direction, which were used in the analysis of the data. Water temperature was obtained by a precision thermometer and a bucket when the boat was stopped. A thermistor located on the boat's bottom displayed the water thermometer reading while the boat was in motion. A standard sling psychrometer was used to measure the dry and wet bulb temperature at a regular schedule. A manual NRL radon counter was used for radon data.

Table 4. Instrumentation aboard the *Renegade*.

Key-90, July 1990		
Parameter	Instrumentation	Institute
Aerosol Size Distribution	Optical Particle Counter	UMIST
	Rotorod Impactor	TNNO – FEL
	Particulate Volume Monitor (PVM)	Gerber Scientific
	CN Counter	PMTC
Boundary Layer Meteorology Profiles	Radiosonde	NPS
Visibility	HSS Visiometer	NRL
Radon Concentration	Manual Radon Counter	NRL
Wind	Sonic Anemometer	UMIST
	Bivane & Compass	NRL
	Manual Anemometer	NRL
	Mini Weather Station	NPS
Air Temperature	Mini Weather Station	NPS
Dew Point and/or Relative Humidity	Mini Weather Station	NPS
	Ophir Hygrometer	UMIST
	CHUM Hygrometer	UMIST
	Psychrometer (Dry/Wet)	NRL
Sea Surface Temperature	Bucket Thermometer	NRL
	Boat Hull Thermistor	NRL
Atmospheric Pressure	Mini Weather Station	NPS
	Precision Barometer	NPS
Optical Depth	Sun Photometer	NRL

PVM, on loan from Gerber Scientific Inc., is a new instrument recently put on the market. In reality, the PVM is a laser-diffraction instrument, and it was used to measure *in situ* either the integrated volume of aerosol particles, or their optical extinction coefficient in the far infrared (Gerber, 1989, 1991).

Meteorological and support measurements necessary to evaluate the model were made aboard the *Renegade* for all days of the experiment. The instruments used are described below in more detail. Three personal computers were used in processing and storing most of the data for later analysis. Whenever possible, manual measurements were also made to serve as a backup to the automatic systems.

UMIST: Aerosol and Flux Measurements

The aerosol particle measurements taken from the boat at a mean height of about 4 m above the surface of the water were made by means of a PMS FSSP–100 (the optical particle counter in table 4), which was installed on an open-framed tower on the bow of the boat. This instrument was

designed for aircraft use, but the UMIST group's experience during cruises in the north east Atlantic and the North Sea under high wind conditions showed it to be well-suited to operate from a boat in the marine environment. This particle counter covered the radius range from 0.25 to 23.5 μm, encompassing all aerosol sizes of interest. It functioned effectively throughout the project, requiring only routine, intermittent attention to remove any salt buildup on the optical components. Presized glass beads were employed frequently during the project to ensure that the laboratory calibration of this device was maintained at all times.

The FSSP-100 was interfaced to a UMIST-developed microprocessor unit that made histograms of the particle counts within its internal memory before it transmitted the resultant spectrum to the data logging computer. This unit cycled through the various probe size ranges and, since the sample time was controlled by the interrogating NRL computer, its sampling time could range from less than one second to periods limited by only integer overflow within the microprocessor unit.

An additional package made high-frequency measurements of vector wind speed and water vapor density. The purpose of this data was to provide wind stress and water vapor fluxes by using the "dissipation" technique. The values of u_* and q_* obtained during the observational periods would be available to assist with the interpretation of the aerosol measurements.

This package consisted of a *Gill* sonic anemometer giving 21 Hz observations of 3-axis wind speed together with two devices for measuring absolute humidity — an Ophir IR hygrometer and a UMIST prototype instrument based upon highly sensitive measurements of the changes in the dielectric constant of air samples associated with water vapor density changes. The UMIST humidity device has shown itself capable of functioning for extended periods at sea during a recent North Atlantic cruise, but it has yet to be fully calibrated in the field.

The Ophir IR hygrometer provides high-frequency measurements of absolute humidity by the differential absorption of IR radiation at 2.5- and 2.6-μm wavelengths. The instrument contains an internal microprocessor that governs its operation and handles the transmission of the output data down a bidirectional serial interface. Various operational modes are selected by sending appropriate signals along this interface from a host computer. At its highest operating frequency of 20 Hz, which is necessary for the dissipation analysis technique, data are presented in the form of pairs of integers representing the raw transmission signals at the two operating wavelengths. This information must be processed externally to provide absolute humidity measurements. At a lower rate of 2 Hz, these transmission values may be internally processed and averaged to produce outputs in various engineering units together with associated observations, such as ambient air and internal instrument temperatures that are required for the external processing of the raw transmission signals. Thus, to operate this hygrometer at maximum speed for the purposes of moisture flux calculations, raw differential transmission signals must be interspersed intermittently with requests for air and instrument temperatures to take account of any drift in the prevailing conditions.

The sonic anemometer possessed a similar serial interface to the Ophir device and, because of the heavy demands placed upon the data handling system by these instruments, they were coupled via a multiserial card to a separate personal computer. The personal computer was programmed to collect more than 2048 data samples at maximum speed (i.e., an overall sample period of almost 2 minutes) from each of the two serial instruments, then read the computer system clock and the CHUM hygrometer, and request air and device temperatures from the Ophir. Calculations using Fast Fourier Transform techniques were then performed upon the collected data to determine the power spectral densities of the anemometer and Ophir hygrometer signals from which values of u_* and q_*, could be determined. After this calculation period of approximately 30 seconds, this cycle was repeated.

While this 2-minute sample period was considered rather brief for meaningful individual values of u_* and q_*, it probably represents a reasonable lower limit to the temporal resolution of the dissipation technique to which further time–domain smoothing may be applied.

TNO's Particle Measurement System

Measurement of particle size distribution in the large particle range was done with a device known as a Rotorod from Sampling Technologies, Inc. Several of these devices were mounted on a spar buoy at various altitudes above the water surface in order to provide profiles of aerosol near the air–sea interface. The Rotorod is an inertial impactor that measures the concentrations of particles with diameters larger than 13 μm. The instrument consists of two polished stainless steel rods that are 8.3 cm apart and are mounted on a motor that rotates at 2400 rpm. The linear velocity of the rods is 10 m per second. Aerosol particles with high inertia impact on the rotating rods. In order to retain the particles, the rods are sprayed with silicon. To prevent particle collection before starting the sampling or after completing a measurement, a retracting collector head system was used. When the sampler started rotating, the rods tipped up due to centrifugal forces, and when the sampler stopped, they were retracted. Sample times were usually set to 4 minutes, which, from earlier experience, appeared to be long enough to get reasonable statistics and short enough to prevent too dense a collection of impactions so individual particles could still be distinguished.

The exposed rods were examined under a microscope. Six images of areas on each pair of rods were chosen at random and photographed through the microscope. Thus, 12 photographs were taken for each sample. Two magnifications were used. Ten photographs were taken with the usual magnification (100x), which visualized particles larger than 10 to 13 μm. This was also the lower cut-off diameter for 100% sampling efficiency with the rods used. Experience has shown that the particle size distributions are reliable for particles in the 13-μm and larger size range. In addition, two photographs were taken with 50x magnification in order to increase the statistics of the larger particles by using a larger sample volume. The photographs were later digitized to determine the size distribution of the collected particles by computer.

The Rotorod impaction sampler has two applications. In the first place, it complements the optical particle counter measurements by extending the size range of the particles that can be measured from 13 μm to 100 μm. Previous experiments showed that the spectra obtained with Rotorod impaction samplers and the PMS optical particle counter (CSAS–100 HV) are in good agreement in the overlapping size range, despite the difference in the physical principles on which they are based (de Leeuw, 1986).

The Rotorod sampler can be easily mounted in places not readily accessible to bulkier and heavier equipment, because of its small dimensions and light weight. Therefore, it is a suitable device for profiling the particle size distributions in the surface layer to very close to the air–sea interface. For this purpose, the sampler is mounted on a simple wave follower consisting of a toroidal buoy that is fastened on gimbals to a bar. A weight—12 kg during KEY-90—was fastened to the bottom of the bar, which extended about 1 m below the buoy, to keep it vertical by gravitation. For stability, the length of the bar extending above the buoy was limited to less than 1.5 m. Consequently, the aerosol size distribution profiles measured from the float were also limited to levels below 1.5 m. For easy servicing, the Rotorods were now mounted on a tube that was slid over the bar that was fastened to the buoy. The Rotorods were mounted on 40-cm extension rods to reduce the influence of the buoy on the measured particle size distributions. This setup is shown in the photograph in figure 4.

The float drifted freely with only a rope and a power cable tied to it. The rope served to haul the float in for replacing the rods. The float was launched when the *Renegade* was at station and drifted with the wind broadside. Since the boat was larger, it moved more easily than the float due to the

wind pressure. Thus, a distance was maintained between the float and the boat by the blowing wind. Measurements were made with the float 10 to 15 m upwind of the boat.

Particle size distributions were measured at four heights: 0.5, 0.75, 1.0, and 1.25 m above the instantaneous water level. Additional measurements were made at a height of about 4 m above the mean water level near the PMS instrument. Measurements were taken only when the boat was stopped at the station.

NOSC AIRBORNE FACILITY

NOSC provided an airborne platform to obtain horizontal and vertical profiles of aerosol size distributions, air temperature, dew point, and sea surface temperature within the marine boundary layer (MBL). The optical properties of the MBL were then determined by using the profiles of aerosol size distributions and Mie theory. Figure 2 shows the airborne platform. Table 5 lists instrumentation packages aboard the aircraft.

Table 5. Instrumentation aboard the NOSC airborne platform.

Aerosol Size Distribution	Optical Particle Counter: FSSP
Aerosol Size Distribution	Optical Particle Counter: OAP
Air Temperature	Rosemont Temperature Probe
Dew Point	EG&G Dew-Point hygrometer
Sea Surface Temperature	Everest Thermometer
Atmospheric Pressure	Rosemont Pressure Transducer
Altitude	Radar Altimeter

Data profiles were obtained by flying spirals at selected geographic locations and constant altitude flights were flown at selected radials with respect to Bonefish Towers. The aircraft flew at altitudes ranging from just off the surface to 4500 m and at an airspeed of 54 m per second. The ascent rate on all spirals was approximately 2.5 m per second. Aerosol size distribution measurements from 0.5 μm to 320 μm were made by using the two PMS spectrometer probes. The spectrometers were operated to allow for a 4-second data sample every 10 seconds (maximum sampling rate for the PDS-400 data acquisition system). The FSSP-100 sized particles from 0.5 to 47 μm into four range bands with 15 channels per band. The spectrometer sequentially stepped from range 1 to range 4 in 4 seconds and digitally output a spectrum during the 6 seconds following the sampling period (one 15-size channel spectrum for each range band). The OAP–200 has only 1 range and is divided into 15 channels. It provided a spectrum from 30 μm to 320 μm during the same 4-second sampling period. By combining the data from each probe and eliminating channel overlap, a 51-bin spectrum from 0.5 to 320 μm could be obtained every 10 seconds. These spectra could subsequently be averaged for any desired time period. Particle density per unit volume per μm interval and cumulative densities greater than or equal to a given diameter could be calculated by using the particle count per unit time, the sampling area, and the aircraft speed. The total scattering, absorption, and extinction coefficients for a given optical wavelength were calculated by integrating the MIE single particle cross sections over the appropriate distribution. All spectrometer data were processed by using the Compaq 386 portable computer. All meteorological parameters were digitally recorded every 5 seconds and subsequently processed by the Compaq 386. The NOSC airborne platform made 18 flights consisting of 42 vertical profiles and 36 low-level, constant-altitude, sea surface runs.

A typical NOSC aircraft flight operation consists of constant-altitude flight going to and from the rendezvous point and spirals above these locations. The constant-level flight is done at a few hundred feet altitude so that sea surface temperature can be accurately mapped. These measurements are most accurate when a minimum amount of air is between the aircraft and the sea surface, because the atmospheric water vapor affects the remote sensing process of the instrument. The spiral maneuver takes about one-half hour and consists of going from very close to the sea surface to about 3000 m in a circling manner. Vertical profiles of air temperature, relative humidity, and potential temperature from the spirals are used as the input meteorological profile data for NOVAM. The aerosol size distributions obtained from the spirals and the long, constant-altitude flights are used as a standard by which to judge NOVAM.

NRL'S AIRBORNE LIDAR

The NRL lidar is an active system that uses light to probe the atmosphere. A short, collimated pulse of infrared light from a laser is aimed directly down from the aircraft through the atmosphere to the ocean surface. A telescope collects the light that is scattered back toward the aircraft. A photo diode in the focal plane measures the direct backscattered lidar signal.

The light reflects off the ocean waves in a wide range of angles. As this light passes up through the atmosphere, aerosols scatter some of it towards the aircraft, forming a bright disk around the reflection spot (much like a corona formed by the moonlight scattering off thin stratus clouds). A second photo diode in the second focal plane of the telescope measures this aureole signal.

The direct reflection (lidar) and aureole signals are used to estimate the optical depth and to provide critical information on the conversion of lidar backscatter into extinction (see Hooper & Gerber, 1986, 1988, as well as the data analysis section for more detail on this process). The time- resolved aureole signal also detects multiple scattering. Although not used explicitly in the data analysis, a multiple-scattering signal shows when the standard single scatter analysis fails. Table 6 shows characteristics and components of this system.

As an adjunct to measurements from the boat and NOSC aircraft, a large-scale map of aerosol variations can be derived from lidar data. Individual lidar profiles have a resolution of 7.5 m. Collectively, the lidar profiles reveal the large-scale variation of aerosol scattering in the atmospheric cross section defined by the flight path (approximately 65 km) and ranging in height from the surface to the aircraft altitude (typically 3 km). Within this cross section, the boundary-layer depth, individual cell size, and cloud height are identifiable.

Table 6. NRL lidar system parameters.

Transmitter:	
Wavelength	1.06 micron
Pulse Duration	8 ns
Energy	750 mJ
Laser Repetition Rate	10 Hz
Beam Divergence	0.5 mrad

Receiver:	
Telescope	Cassegrainian, 32 cm diameter
Detectors	Silicon Avalanche Photo Diode
Field of View (Lidar)	1 mrad
Field of View (Aureole)	30 mrad

Acquisition Systems:	
Digitizer (Lidar)	20 MHz, 12 bit
Digitizer (Aureole)	100 MHz, 10 bit
Averaging (Typically)	20 wave forms
Acquisition Computer	PDP-11
Display	Compaq 286, PGA monitor 256 colors, 480x640 pixels
Storage	Bernoulli disk 40 Mbyte

INSTRUMENTATION ASHORE AT MARATHON, FLORIDA

Shore-based instruments were used during these operations. A basic set of meteorological data was taken in the vicinity of the multistory building that housed the TNO lidar. An automatic radon instrument was also located in the building and exposed to outside air. Some radiosondes were taken at the dock where the *Renegade* was based as well as at the rendezvous point. These measurements were used to determine if an island heating effect that could influence the interpretation of the shore-based lidar existed between water and land. Finally, the wind was measured on a continuous basis at the Marathon airport. These data were used to determine the 24-hour average wind. Due to the existence of the sea breeze and other diurnal processes occurring here, an extensive statistical study was done to relate the measured wind at the airport and the more spotty wind measurements made at the rendezvous point by the instrumentation on the boat. These data were used in conjunction with the

correction parameters determined from this study in order to obtain the average 24-hour wind speed used in the surface observation files of NOVAM. Table 7 summarizes the various island measurements made during KEY-90.

TNO Mini Lidar

The TNO mini lidar (wavelength 1.06 μm) is a modification of an Oldelft Optical Industries (Delft, the Netherlands) military laser range finder. The modifications include changes in both the optical and electronic parts of the system.

Table 7. Measurements made on shore during KEY-90.

Boundary-Layer Profiling	TNO–FEL Mini Lidar	TNO–FEL
	Radiosonde	NPS
Air Temperature	Micro Weather Station	TNO–FEL
Relative Humidity	Micro Weather Station	TNO–FEL
Atmospheric Pressure	Micro Weather Station	TNO–FEL
Radon	Automatic Radon Counter	NOSC
Wind (At Airport)	Anemometer	NOSC

The heart of the lidar is an Nd:glass laser with a rotating prism as a Q-switch. The elevation angle of the laser beam is adjustable with an internal mirror and can be varied from angles of about −10° to about +33°. During the KEY-90 experiment, the lidar was mounted at an angle of 30°, thus changing the maximum elevation angle to 63° to enhance the vertical range.

The receiver consists of an optical telescope that focuses the backscattered laser light on the photo diode. Background radiation is suppressed by an RG830 color filter. A logarithmic amplifier (Optech OS-LA-5-20) has been applied to suppress the dynamic range in the signal. This unit has a logarithmic transfer over the first 80 dB of the input signal (0 dB = 3 V) and a constant transfer for smaller ($< 3.10^{-4}$ V) input signals. The advantages of this unit, as compared to other log amplifiers, are the large dynamic range of at least 100 dB at the input and the large electric bandwidth of about 40 MHz (6 dB).

The whole lidar system is controlled by a personal computer (PC) via an IEEE-488 bus (National Instruments). The data are recorded by a dual channel transient digitizer (Tektronix 7612). During KEY-90, one channel was used to record the boundary-layer return signals from a maximum range of 2600 m (resolution 3 m), corresponding to a maximum height of 2250 m at a 60° elevation. Using a pretrigger, the first 160 samples provided a reference level for the lidar return signal. The other channel was used for monitoring cloud reflections up to a 13-km altitude. This information was used only to obtain information on the altitude of very high cloud layers, and this altitude information was manually recorded in the logs. These cloud layers were only occasionally seen during the TNO – FEL observations (we estimate that they occurred 1 to 5 % of the time).

The maximum range of the TNO mini lidar is determined by the energy of the laser, the diameter of the receiver, and the noise of the detector, as well as the actual weather. It was between 1.5 to 2 km during the KEY-90 experiments.

The lidar was mounted on the 8th floor (about 25 m above sea level) of a high-rise apartment building known as Bonefish Towers, which is about 150 m from the beach of the Straits of Florida.

The pointing direction of the lidar was about 170° with respect to north. The elevation angle was fixed at 30° from the horizontal plane. The wind was generally from the southeast (i.e., onshore, toward the lidar). Figure 3 shows the lidar system as it was mounted during the KEY-90 experiment.

THE WAVE BUOYS

Two waverider buoys, manufactured by Datawell were used for wave height measurements. The buoys employed an accelerometer to monitor their vertical acceleration, providing a measurement of the vertical displacement of the sea surface as a function of time. This information was transmitted at 28 MHz to a receiving station at Bonefish Towers, then digitized on a PC. The buoys were located on approximately a 169° (true) bearing from Bonefish Towers (latitude 24°43.4', longitude 81°00.07') at the positions listed in table 8.

Deployment was on 6 July (Julian date 187) and data were collected nearly continuously thereafter. Buoy 2 operated until the end of the test on 19 July (14 days). Buoy 1 was accidentally set adrift from its mooring at approximately midday on July 10 and its position after midday 10 July was uncertain.

Table 8. The buoy positions.

	Latitude	Longitude	Distance from Bonefish Towers	Sea Depth
Buoy 1	24°36.0' N	80°58.3' W	11.4 km	400 ft
Buoy 2	24°39.2' N	80°59.6' W	6.7 km	100 ft

DATA OVERVIEW

During the 3-week period, a separate experiment was carried out every day except Sundays and the Fourth of July holiday. Not all individual instruments were operating every day of the experiment because of the problem of getting all instrument systems up and running and keeping them up and running throughout the experiment, However, on those days when some instruments might have failed for some reason, the experiment was still a success because at least one measurement was made of every input parameter to NOVAM. Table 9 shows that all surface observation file inputs to NOVAM were available for all the days of operation.

The KEY-90 experiment coordinated profile data that NOVAM needed from the NOSC aircraft, the NRL aircraft, and the radiosonde flights with the surface observations from the boat. It must be remembered that when a rendezvous point was picked for the operation, the time for the boat to travel between the dock and the point was considerably greater than the time required for the aircraft to go from the local airport to the point. Although the boat obtained data while in transit to the point, the best surface data for any day occurred while the boat was on station, either stopped dead in the water (ideal for wind measurements) or making a very slight headway into the wind to obtain the best sample for the aerosol samplers. The aircraft would usually wait until the boat was on station or almost on station before it would proceed to the rendezvous point. Caution was used when trying to make an aircraft profile while launching the radiosonde. Attempts were made to execute the two profiles close together but on only two occasions (when visibility was excellent) did the balloon radiosonde and the aircraft measure their profiles at the same time. In addition, a post-experiment radiosonde was launched from the dock in Marathon on three occasions.

Table 9. Days when observation systems were operational in KEY-90 showing redundant measurements of data essential for inclusion into the NOVAM surface-observation file.

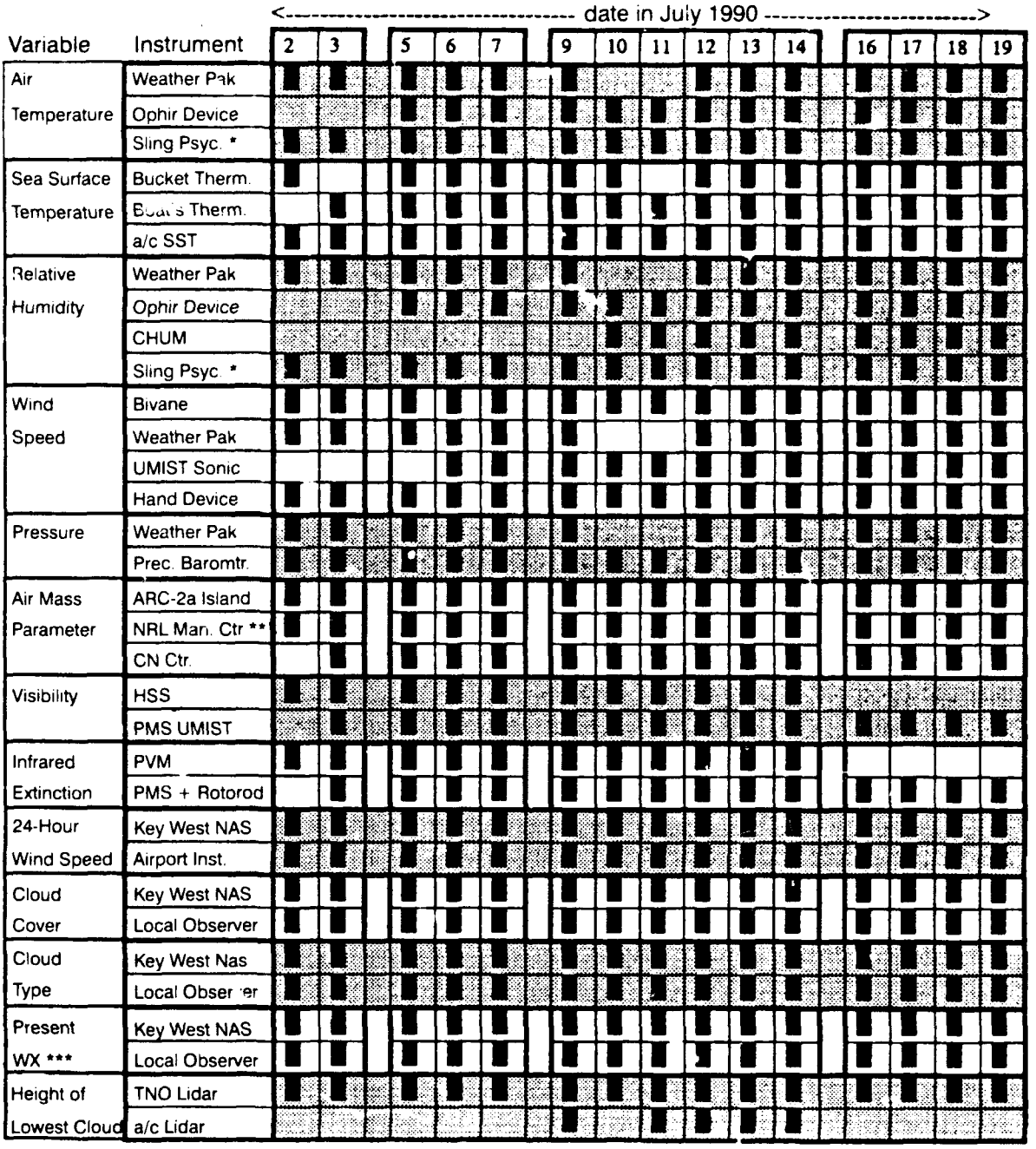

* Psychrometer
** Manual Counter
*** Weather Observations

OVERVIEW OF TNO – FEL DATA

During the first few days of the experiment, the shore-based lidar time of operation was synchronized with the times that measurements were made from the boat. Later, the periods were extended to between 8 and 12 hours to study the temporal variability and the forecasting capability of NOVAM and to overlap the boat measurements. The lidar operated most of the time at a repetition rate of 3 per minute for observation of the dynamical behavior of the boundary layer. Table 10 gives an overview of the periods during which lidar data were recorded. The subsequent weeks were separated by a 24-hour time axis. For details on data storage, its availability, and a survey of preliminary results, see de Leeuw et al. (1991).

AIRBORNE LIDAR

The time when the NRL airborne lidar was operated was limited by both cost of operation and the availability of flight time. The KEY-90 experiment was fortunate because the P3 aircraft was in Florida during the midperiod of the experiment when the other systems were in full operation. Table 11 shows the actual times when the lidar was flown.

Table 10. Local times when the TNO island-based lidar was in operation.

date ⇓ ⇐ Time E.D.T.⇒

	0	1	2	3	4	5	6	7	8	9	0	1	2	3	4	5	6	7	8	9	0	1	2	3
2											■	■	■	■	■	■								
3												■	■	■	■					■	■	■	■	■
4																								
5											■	■	■	■	■	■	■	■	■	■	■	■	■	■
6												■	■	■	■	■	■							
7										■	■	■	■	■	■	■	■	■						
8																								
9															■	■	■	■	■	■	■	■		
10															■	■	■	■	■	■	■	■		
11																	■	■	■	■	■	■	■	■
12													■	■	■	■	■	■	■	■	■	■	■	
13							■	■	■	■	■	■	■	■	■	■								
14					■	■	■	■	■	■	■	■	■	■	■									
15																								
16															■	■	■	■	■	■	■	■	■	■
17												■	■	■	■	■	■	■	■	■	■	■		
18							■	■	■	■	■	■	■	■	■	■	■	■	■	■	■			
19					■	■	■	■	■	■	■	■												

Table 11. Times when NRL aircraft lidar was in opeation.

date ⇓ ⇐ Time E.D.T.⇒

	0	1	2	3	4	5	6	7	8	9	0	1	2	3	4	5	6	7	8	9	0	1	2	3
8																								
9																	■	■	■	■				
10																								
11																				■	■	■	■	
12															■	■	■	■						
13										■	■	■	■											
14							■	■	■	■														
15																								

PRELIMINARY DATA ANALYSIS

GENERAL COMMENTS

Due to the very large amount of data available from KEY-90, this report will not attempt a complete analysis, but will serve as a reference that can be consulted as more detailed data are published. However, because of the vast scale of the data taken, the various authors felt it would be desirable to examine a case study for a particular day when most of the instrumentation was operating and which could be considered somewhat typical of the experiment. Consequently, 14 July 1990 was chosen as the day. The data that follow are aimed at testing NOVAM on that particular day, but many other observations might be made from the data on this and other days. For instance, on 14 July 1990, a good possibility of comparing the extinction profile obtained from the aureole lidar with an *in situ* profile of aerosol size distribution could be made. An extinction from the measured aerosol size distribution at the lidar's wavelength could be calculated via Mie theory for this comparison.

On this day, a redundancy occurred in most of the measurements and especially in the data for the NOVAM input files. This section of the report will describe the methods by which a consensus of multiple data was obtained for the testing of the model.

In the following portion of this section, we will describe the various aspects of the data for 14 July 1990 as taken during the KEY-90 experiment. We will first look at the general weather situation, how the two input files for NOVAM were generated, the turbulent parameters data, the wave data, the surface aerosol measurements, and the lidar measurements for this period.

ATMOSPHERIC SYNOPTIC SCALE ANALYSIS

The major synoptic flow patterns that influenced conditions in the marathon region from 9 to 19 July are shown in figure 5. For the period of 9 to 19 July, surface winds at Marathon were generally from the east to southeast with speeds of approximately 5 meters per second (m/s). This was a result of the influence of high pressure centered off the east coast of the U.S. (figure 5a). The high-pressure system continued to control the Marathon region winds on 11 and 12 July. However, short-wave troughs were analyzed as passing through Marathon on 11 July.

As the high-pressure system moved to the northeast, winds at Marathon shifted from east-southeast to a more southerly direction (figure 5b). Wind speeds were between 3 and 5 m/s during this period. By 13 July, a low pressure system that was approaching the eastern U.S. influenced winds at Marathon. Wind flow remained southerly, but wind speeds decreased slightly due to a weaker pressure gradient over the area. On 14 July, the low-pressure center had deepened and moved to the east (figure 5c). Surface wind flow over Marathon remained southerly with wind speeds increasing to 6 to 8 m/s. The cold front associated with the low-pressure system was moving very slowly to the east. By late on this day (14 July), it was evident that the frontal system was losing its upper level support, and the high pressure evident at 700 mb near the Florida Keys (figure 5c) continued to build.

From 15 to 19 July, high pressure once again dominated the flow pattern in the Marathon region (figure 5d). As the high-pressure center moved to the north-east, the pressure gradient weakened at all levels. Surface winds were from the east to southeast throughout this period, with wind speed decreasing to approximately 5 m/s by 19 July. A series of short-wave troughs was analyzed as passing through the Marathon region on 17 July.

Although all observations made during KEY-90 fell within the realm of weak convection defined by NOVAM, there were examples of deep convection in the form of thunderstorms. Thunderstorm activity was observed in the Marathon region on 14, 16, 17, and 19 July.

GENERATION OF THE CONSENSUS SURFACE DATA FILE

The consensus surface data values for each day are listed in the appendix of this report. A good deal of statistical analysis of this data has been done to ensure the best possible set of numbers to represent what actually happened at the boat during the KEY-90 experiment.

The sea-surface temperature (SST) data on the consensus tables were taken while the boat was on station—both while heading into the wind and stopped. The boat hull thermometer data were corrected by means of a linear correction factor (obtained from a regression line determined from all the KEY-90 data in which the bucket temperature and the boat hull thermometer were measured simultaneously). In this case, the bucket temperatures were considered to be the correct value, but the hull temperature could be obtained much more rapidly. After correction, both types of data could be used in the average calculation. Additional SST data were taken from the NOSC aircraft by means of an IR sensor while the aircraft was making the lowest 200 m of the various profiles. Data from those spirals near the boat were also used in the averaging process. It was also assumed that the SST did not change much from hour to hour, so a delay between measurements was not considered significant. Although the aircraft-derived SST values were "skin" temperature and the boat SST values were "bulk" values that differed from each other physically, we assumed that these differences were not crucial in the testing of NOVAM. Thus, equal weights were given to each observation to arrive at the consensus value. In looking at other aspects of air–sea interaction, this assumption may not be accurate.

The air temperature (TAIR) data were the extrapolation of the potential temperature measurement taken from the aircraft over the lowest few hundred m and the air temperature measurement from the Weather Pak. Temperature measurements from the Ophir device and the manual instruments on the boat were not included in the consensus data, because they showed signs of containing an insolation factor apparently caused by insufficient sun shielding of the apparatus. The radiosonde potential temperatures at the lowest levels were not used because of a large inconsistency noted between some of these sondes and the other devices.

The relative humidity (RH) data in the consensus surface observation data files were obtained with the same technique used for the TAIR data. Here again, none of the radiosonde data were used

since these data, although adequate for relative values needed in the sounding, were not really as accurate for single point measurements as the other devices. During the KEY-90 experiment, the Ophir hygrometer did not seem to be working properly, giving apparently erroneous data most of the time. This data source was not used in the consensus data file. At the time this report was prepared, a satisfactory algorithm for the UMIST CHUM device was unavailable, and therefore data from this device were not used in the statistical calculation of RH for the surface observation file. Low-level NOSC aircraft humidity measurements that were extrapolated to boat level, the Weather Pak on the boat, and the manual sling psychrometer were used to obtain these, onsensus data.

The visibility input to the surface observation file came from both the boat-mounted HSS visiometer and Mie calculation of the aerosol size distribution measured on the boat for a wavelength of 0.55 μm. Data from the aerosol size distribution measured at its lowest level of spiral near the boat by the NOSC aircraft were also used as a source of aerosol for Mie calculations in order to contribute to the visibility data used in the surface observation file.

The instantaneous windspeed (WS) data were obtained directly from the boat data for the period when the boat was stopped. It contained the means of the bivane anemometer, the Weather Pak vector windspeed, a manual windspeed measurement, and the mean from the UMIST sonic anemometer. Windspeed seemed to be one of the best measurements because the scatter between different instruments appeared to be the least. Separate, independent, windspeed measurements were used for each location during week 3, when experiments were performed at two different locations on the same day.

The 24-hour average windspeed data (WS24) for these periods were obtained from an anemometer that operated at the airport in Marathon. These data were recorded every minute and the anemometer was in operation for 24 hours a day. The relationship between this measurement and the windspeed over the sea at the rendezvous point several miles away was necessary for the consensus data file to be completed accurately.

At least two effects will cause two anemometers to differ from each other, even if both the boat and the island were hypothetically exposed to exactly the same wind. The first effect is the sea breeze, which is a diurnal effect that will cause a diurnal variation to the island-based measurement. This should not affect the measurements at sea (assuming that the boat is far enough away from land). The second effect is a constant offset related to the orientation of the instruments. Presumably, the instrument on the island will have some distortion because of buildings, trees, etc. Therefore, in order to use the 24-hour windspeed monitor, the corrections to these two known effects must be taken into account. The removal of the sea-breeze effect is relatively easy, because the effect is quite pronounced in the hourly averages of the airport data plotted as a function of time of day (figure 6).

A variation in windspeed of almost 1 m/s was observed over the 20-day averages obtained for KEY-90. A correction factor was then applied to each of the observations to account for this diurnal effect. The next approach was to find some factor by which to multiply the corrected island windspeeds in order to obtain the winds observed at sea on the boat. This method will obviously have a considerable amount of variation. However, a regression was found that related the island wind to that which we would expect at the boat. We could then construct the windspeed at the boat by using the measurement at the island. The actual set of measurements at the boat were compared with the constructed windspeeds obtained from the data simultaneously measured from the island and plotted in a scatter plot form in figure 7. While there was a fair amount of scatter here, the corrected winds were a significant improvement over using just the measured windspeed from the island. We saw then that within a certain amount of error, we could estimate the wind at sea for time when the boat was there, and therefore the estimate of it should have been possible even when the boat was not

there. This logical step was necessary so that the average windspeed over the water could be calculated even if the boat had not been on station for the full 3 weeks of KEY- 90. The final step was to use these reconstructed windspeeds to estimate a 24-hour average wind from the measurements on the island. This was done and the WS24 data for KEY-90 are shown in the table in the appendix.

The air mass parameter for the surface observation file was obtained from the radon 222 measurements made at the land site in Marathon and from the radon measurements made aboard the *Renegade*. The relationship was originally given by Gathman (1983 a,b) as **a.m.p. = Rn/4 + 1**, where Rn is the radon 222 activity expressed as p Ci /m^3.

The cloud cover (cc) and the cloud type (ct) data were obtained from the weather observations made by the participants of KEY-90 as well as from the weather office at the Naval air station in Key West.

The surface extinction input value at 10.6 μm may not always be available when using NOVAM. However, in this "best" case test of NOVAM, it was available and was calculated from the aerosol size distribution data taken from aboard the *Renegade* (figure 8) and from the lowest level of the associated NOSC aircraft spiral by using Mie theory.

The present weather (pw) parameter used by NOVAM was obtained from notes taken by the local observers at both the island station and the boat as well as by the aircraft people. The level of the parameter "lowest cloud level" (zcld) was obtained from the observations of the NOSC aircraft crew.

The data from these sources were compiled together to form the consensus data file and were used for all NOVAM calculations related to the KEY-90 experiment.

GENERATION OF NOVAM'S METEOROLOGICAL PROFILE FILES

The meteorological data taken on the aircraft and the meteorological profiles obtained from the radiosonde ascents were compared with each other. The comparison for the 14 July 1990 data is described in detail in the "discussion" section. For each flight, a preamble was determined and inserted into the front of the meteorological profile data *expressed in altitude, potential temperature, and mixing ratio*. This was the meteorological profile data file used to run NOVAM.

MOMENTUM AND MOISTURE FLUX MEASUREMENTS FROM THE *RENEGADE*

An additional package of instruments was installed by UMIST on the boat in order to provide high-frequency measurements of vector windspeed and water vapor density, so windstress and water vapor fluxes could be determined by means of the dissipation technique. The calculation took place over an observation period of 2 minutes. The values of u_* and q_*, which were obtained during the observational periods, were available to assist with the interpretation of the aerosol measurements.

While this 2-minute sample period was considered rather brief for meaningful individual values of u_* and q_*, it probably represents a reasonable lower limit to the temporal resolution of the dissipation technique to which further time–domain smoothing may be applied. This was probably the cause of the jitter in the u_* values shown in figure 9.

WAVE MEASUREMENTS DURING KEY-90

The wave buoys were in operation and sending their data back to shore during much of KEY-90. Although both the power spectrum density of the wave activity and the root mean square (rms) heights of the waves are available from the data set, only the rms data and the windspeed data in figure 10 (which shows a definite relationship between rms wave heights and the wind) are included

here. Some marine aerosols are produced by the bursting of air bubbles at the sea surface. The bubbles are introduced into the sea by white-capping phenomenon and are related to various aspects of the waves and wind. An interesting feature of this data set is the comparison between the rms wave heights (figure 10) and the aerosol size spectra (figure 8) on 13 and 14 July 1990 (Julian days 194 and 195) during KEY-90. On 13 July, there was a decrease in the rms wave height values during the day, while there was a low concentration of aerosol sizes between 0.5 and 10.0 μm. In contrast, rms wave height values increased by the next day, with a corresponding higher concentration of aerosols throughout the spectrum as would be expected. Obviously, the scope of this report does not allow us to investigate the statistics of the wave – aerosol concentration relationship with such a small amount of data. Many factors are missing in this relationship, and this case study does not begin to cover, in detail, the physics of the breaking waves and the dependence on wind, etc. There is even some evidence of the seawater temperature being a parameter to watch in terms of aerosol production.

AEROSOL MEASUREMENTS FROM THE *RENEGADE*

For the KEY-90 project, a basic aerosol sampling period of 10 s was selected to provide appropriate temporal resolution. However, the stored spectra have subsequently been integrated over longer periods to improve the sampling statistics.

Compared with most other UMIST marine aerosol investigations, winds were generally much lighter and preliminary analysis of these data suggested that the prevailing windspeed was much less dominant in determining the aerosol loadings. High air and sea temperatures, which consequently have high-water vapor concentrations and relative humidities, probably did much to modify aerosol particle spectra. In addition, frequent thunderstorms and large convective cells obviously played a significant role in removing particulates from the atmosphere and thus in modifying the observed spectra. These points are illustrated in the samples of aerosol data shown in this report.

On Thursday, 12 July 1990, heavy thunderstorms were active in the area. By 13 July, they had cleared and exceptionally good visibility and calm conditions with windspeeds of around 2 m/s existed. Particle concentrations on 13 July were very low, as shown in figure 8, with counts of less than 60 per liter over the radius range from 1 to 16 μm. Even after integrating the particle counts over periods of almost one hour, the resultant spectrum exhibited noticeable statistical variability.

An early morning run to investigate the possibility of particle concentration variations associated with sunrise was undertaken on 14 July. Winds at around 6 to 7 m/s, were somewhat fresher than on the previous day, with particle counts consequently about an order of magnitude greater. The boat was on station at 0540 and 0647, approximately one hour before sunrise (0647). Figure 11 shows the temporal variations in aerosol concentration for the two hours around sunrise.

It may be noted from figure 11 that there was considerable variability in particle concentration throughout this period, with a very dramatic increase at sunrise, followed by a fall to lower values, then a subsequent further sharp peak about an hour later. During the period leading up to sunrise, there was substantial cloud cover with some large cumulus cells to the east. The sunrise was not expected to have any direct effect upon the aerosol loadings. Shortly after sunrise, the sky above the boat cleared almost completely, and it is suggested that the lower particle counts were associated with the subsidence of relatively aerosol-free air in the region between the surrounding cumulus cells. However, no convincing explanation for the observed sharp peaks in aerosol particle concentration can be given at the present time. The aerosol particle spectrum integrated throughout this period (figure 8) demonstrates the increase (by almost an order of magnitude) in aerosol loadings compared with the similarly measured loadings from the previous day.

Two size distributions of particles larger than 5 μm in radius were measured with the Rotorod samplers on 14 July 1990 at 0557 and 0642. The particle size distributions changed significantly

during the two hours between the first and the last measurement. The particle size distributions shown in figure 12 were measured by Rotorods from beside the UMIST optical particle counters at a mean height of 4 m above the surface. The concentrations of the smallest particles were quite similar, but for particles of 16 μm the concentrations increased one order of magnitude! Larger particles were not observed in the first sample, whereas in the latter one, 14 and 3 particles were sampled in the 21- and 28-μm radius bins, respectively.

Figure 13 further illustrates the temporal variation of the particle concentrations at 4 m, while figure 14 illustrates the relative humidity and the windspeed. The temporal fluctuations were similar for all sizes, although the relative variations were somewhat smaller for the 8.5- and 12-μm particles (factor 2 or less) and at their largest for the 21-μm particles (more than a factor of 3). These fluctuations were much larger than the statistical uncertainties in the particle concentrations, which were less than 25% for all data shown. From the similarity in the behavior of the concentrations of all sizes, it can be inferred that the particle size distributions shifted as a whole to either smaller or larger sizes, depending on the conditions. Some of these changes can be understood from the variations of the relative humidity, which fluctuated between about 76% and 83% during the measurements.

In particular, the variations in the particle size distributions during the first hour were apparently fairly well correlated with the actual humidity values (compare, for example, the concentrations and humidity values at 30, 45, and 60 minutes). However, the humidity fluctuations were too small to completely account for the observed changes in particle concentrations. In addition, during the second hour, the concentrations of the smaller particles were fairly constant, despite the fact that the largest humidity differences (7%) were experienced during that period.

The particle concentrations' different sensitivities to humidity changes in the first and the second hour could be due to the hysteresis effect, i.e., the growth and evaporation curves of the sea-salt particles with increasing and decreasing humidities are not equal (e.g., Winkler & Junge, 1972). As a result, when humidity decreased, the particles were generally larger than when humidity increased. During the first hour, the relative humidity fluctuated between 79% and 83%. At the times the samples were taken, the relative humidity was about 80%. After 60 minutes, the relative humidity reached its maximum value of 83%; it then decreased to the lowest value of 76%. The deliquescence point of sea salt is about 75%, i.e., lower than the humidities experienced during the present case. Hence, all particles were activated. However, as mentioned above, the variations in relative humidity were too low to explain the observed concentrations in particle concentrations.

Other effects should be considered to account for the particle-concentration fluctuations. These effects are the sampling method and turbulent mixing. A sampler mounted on a small boat at an average level of only 4 m above the sea surface experiences appreciable height variations due to the rolling action of the boat. As a consequence, particles are collected; in this case (with windspeeds of 6 to 8 m/s) particles were collected over a height range of a few m. Thus, the measured particle size distribution represents the mean value from close to the wave tops to several m above. For a well-mixed surface-layer aerosol, such data are still representative for the mean height. However, when a strong surface-layer gradient exists, our measurements at a mean height of 4 m are not representative for this level. Apparently this was the case during the beginning of the measurements, when not only the concentrations were low but also significant gradients were observed in the lower 4 m. (See figure 15 and note that the 12-μm particles are missing in the spectrum taken at 4 m.) This profile was measured between 0545 and 0557. The profiles for particles of 6.5 to 16 μm showed that the gradients were stronger as the particles were larger. Note that the data at 4 m were concentrations measured from the boat and were average values over a range of heights, as explained above. The other concentrations were measured on the wave-following buoy. Therefore, the gradients were likely

larger than those inferred from these data. Unfortunately, no data for intermediate heights, which could confirm this conclusion, are available.

The profile in figure 16 was measured between 0745 and 0755 a.m. on 14 July. Note that the statistical errors for the 28-μm particles were large because only 1, 2, and 3 particles were counted for heights of 1.25, 0.75, and 0.5 m, respectively. The statistical reliability of the other concentrations was 20% or better. In this sample, the gradients were negligible for particles smaller than 12 μm. The gradient of the 16-μm-radius particles was likely larger than could be inferred from the data, as explained above for the profiles in figure 15. This effect was expected to be more obvious for the 21-μm particles. However, this was not supported by the observations. On the other hand, where the measured concentrations for these particles displayed a strong gradient at the lower levels, the gradients for the smaller particles are negligible. The variations in the particle concentrations at levels between 0.5 and 1.25 m were too small to infer any conclusions about the wave-rotor mechanism (de Leeuw, 1990).

The higher concentrations and the smaller gradients at 0755 (figure 16), as compared to those earlier in the morning (figure 15), indicated that the particles were better mixed. Unfortunately, we do not have a meteorological or aerosol history of the hours preceding the experiments under discussion. The logs indicate that the wind picked up and that whitecaps were occasionally observed. This is in line with the meteorological data recorded on the *Renegade* during the experiments on the preceding days. The windspeed recorded on 13 July was about 4 m/s; on 12 July the wind was lower. Not much aerosol could have been generated by such low winds. In addition, the aerosol concentrations could have been further depleted by washout during rain showers. This agrees with the observations. The aerosol concentrations measured in the afternoon of 12 July for aerosol up to 8.5 μm were higher than or similar to those shown in figure 15 for the larger particles. On 13 July, however, the concentrations were lower than those in figure 15.

Careful examination of the island windspeed data shows that the wind began to increase shortly before the experiments started on 14 July. This could explain the very low concentrations observed in the first samples (figure 15, and data points at t = 0 in figure 14). The higher concentrations at later times were due to both generation and turbulent transport. This conclusion is supported by the small differences in the concentrations of the smaller particles in figures 12 and 13 as opposed to the large variations in the concentrations of greater particles in the initial phase of the measurements. During increasing wind, the wave phase velocity and the wind speed were not in balance. This resulted in a higher drag, steeper waves, and more whitecaps. Under these conditions, more aerosol particles were produced.

LIDAR AND METEOROLOGICAL OBSERVATIONS AT BONEFISH TOWERS

On 14 July 1990, the TNO mini lidar operated continuously from 0400 to 1400 EDT. The repetition rate was about 2 shots per minute. Data were recorded over a total range of about 3 km. Above 1750 m, no aerosol backscatter was detected. The height of the mixed-layer and the top of the entrainment layer were determined by analysis of false color lidar plots. The air temperature, the relative humidity, and the pressure were manually recorded from a small meteorological station on the balcony of the apartment. A record of the general weather situation was kept every 30 minutes.

Meteorological Data And General Description Of The Weather At The Island Lidar Site In Marathon

The meteorological data were measured at an altitude of about 25 m above sea level. Figure 17 shows an overview of the variations in temperature, pressure, and relative humidity at the lidar site. The times of the radiosonde launches as well as the time when the airplane passed Bonefish Towers

are indicated. Prior to the official sunrise at 0647, there was sufficient light to illuminate the sea, the horizon, and the surroundings.

Figure 17 shows some temperature fluctuations during the first 4 hours, with a rather sharp rise of about 1°C between 0815 and 0900. The relative humidity fluctuated slightly around a value of 95% before sunrise, then dropped by about 1%. Note the sudden drop in relative humidity at 1030. Within an hour it had dropped below 88%. From this time to 1400, the relative humidity decreased slightly to 87%. The time delay between the temperature jump of 1°C and the drop in relative humidity of 8% was about 2 hours. The general weather situation was quite variable; huge and heavy cumulus towers with sharp ceilings were alternated by cirrus clouds and periods of clear sky.

Lidar Results

The lidar data (1231 profiles) was converted to absolute backscatter profiles by ignoring the transmission losses. This assumption is justified because the visibility was always better than 18 km (estimated extinction @ 1.06 μm is smaller than 0.05 km^{-1}). This would, in the extreme case, require a maximum correction of 18% at the far end (2 km). The assumption that the extinction profiles can be obtained from the backscatter profiles by using a fixed ratio of 0.1 between backscatter and extinction was used in this analysis. The extinction coefficients thus calculated were similar to the results of the NRL lidar.

Figure 18 shows the variation in time of the 2-minutes averaged backscatter coefficients at an altitude of 80 m. The rise in the backscatter coincided with the temperature increase, while the strong decrease in the backscatter after 0930 occurred almost simultaneously with the period when the relative humidity dropped (cf. figure 17). The decrease in backscatter could have been caused by the evaporation of aerosol particles in response to the decreasing humidity. The rise in the backscatter between 0800 and 0930, which occurred simultaneously with the increase in temperature, is not readily understood. At the same time, the windspeed picked up although whitecaps were not observed until later in the day. Nevertheless, the increasing wind might have caused some additional aerosol production, resulting in the backscatter increases.

Mixed-Layer Height and Top of the Entrainment Layer

The mixed-layer height and the top of the entrainment layer, as defined below, were determined from 10-minutes averaged backscatter profiles and the standard deviation of the profile. Examples of such profiles are given in figures 19 and 20. The profiles of the standard deviations provided information on the degree of mixing versus altitude. Small standard deviations occur above the mixed-layer and at low altitudes where the atmosphere was well-mixed. From altitudes of about 100 m to the top of the mixed-layer, the standard deviations increased with altitude because of the mixing with clear air from above. The standard deviations reached a maximum in the entrainment layer. This process has been described, for example by Hooper and Eloranta (1986).

The mixed-layer height and the top of the entrainment layer were determined according to the following procedures:

1. In the case of a clear atmosphere (figure 19): The mixed-layer height was chosen as that height just below the point where the backscatter decreases significantly and the gradient in the average backscatter is still zero. The top of the entrainment layer was determined at the position where minimum backscatter is combined with the minimum in the standard-deviation profile after the sharp (last) maximum.

2. In the case of a cloud or clouds (figure 20): The mixed-layer height was defined at the position where the average backscatter starts to increase just before the cloud reflection. The top of the

entrainment layer was defined at the first minimum in the standard-deviation profile after the last cloud reflection.

The results are shown in figure 21. The mixed-layer height (bold solid line) varies between about 330 m and 550 m. The entrainment layer height, indicated by the thin solid line, is between 50 and 300 m above the mixed-layer height (except in the cases of cloud reflections before sunrise).

DATA ANALYSIS OF AIRBORNE LIDAR

While the various *in situ* measurements were being made from both the boat and the NOSC aircraft, our understanding of the mechanism in operation was greatly improved by the added ability to examine the same atmospheric boundary layer with the two remote-sensing techniques. The shore-based lidar provided the long-term observations of various structure parameters in the general vicinity, but it was unable to look at the same air that the other instruments were measuring. On the other hand, the airborne downward-looking lidar from the NRL aircraft provided simultaneous observations with the *in situ* measurements as well as an overview of the geographical extent of the boundary-layer structure. It was not, however, able to give long-term observations because of the expense in aircraft operations.

The airborne aureole and lidar signals were measured by the NRL lidar. The aureole signal provides information on forward scattering in the atmosphere. The lidar detector observes both backscattered signal from atmospheric aerosol and from the reflection off the sea surface. The aureole and lidar signals combined yield an estimate of the boundary-layer optical depth:

$$\tau \equiv \int_{r'=0}^{r} \sigma(r')\, dr' = \frac{\mathbf{K}(\mathbf{A} - \mathbf{A}_0)}{\mathfrak{R} - \mathfrak{R}_0}, \tag{1}$$

where τ is the optical depth from the aircraft to the surface, **r** is the range from the lidar, and σ is the volume extinction coefficient. **K** is a calibration constant (that corrects for the different efficiencies of the different focal planes and detectors), $\mathfrak{R}$ is the surface reflection signal (lidar), $\mathfrak{R}_0$ is the sky background (lidar), **A** is the aureole signal, and $\mathbf{A}_0$ is the aureole sky background.

The lidar equation relates the power observed by the lidar detector to atmospheric extinction and backscatter cross sections:

$$P(r) = \frac{k\beta(r)}{r^2} \exp\left[-2 \int_{r'=0}^{r} \sigma(r')\, dr'\right], \tag{2}$$

where **P** is the power returned; **k** includes system constants, overlap function, and some scattering characteristics, and β is the volume backscatter coefficient.

An inversion of the lidar return signal is necessary in order to relate atmospheric extinction and lidar – aureole signals. This is a problem area in the full utilization of lidars to remote sensing of propagation parameters. The inversion method used in reducting the data for this report is beyond the scope of this report, but it utilizes the techniques referred to by Hooper and Gerber (1986). The inversion assumes, however, a power–law relationship between backscatter and extinction. For this analysis, a constant backscatter-to-extinction ratio for each profile is determined by using the simultaneous optical depth measurement. In the end, a relationship that expresses extinction $\sigma(r)$ to be some function of the lidar return signal $P(r)$ is obtained. Despite the problems introduced by the

assumptions used in the inversion process, atmospheric conditions during the KEY-90 experiment should have reduced the inherent errors. Estimating random errors in the extinction from random variability between lidar profiles suggests that the errors in extinction were approximately 20%.

Assuming the inversion process is not too much in error, the instrument allows us to look at the marine atmosphere in a way that can be very useful in understanding the temporal and spatial variations taking place in this convective environment. The data will be presented in a way that will make these variations apparent so they can be used in our evaluation of the model. First of all, with the downward looking lidar, the atmospheric layer under observation is between the plane and the ocean surface. A level-flying aircraft's distance between the lidar and the ocean (that is the aircraft height) can be very accurately determined by the system, because the ocean surface is such a very prominent feature in the lidar returns, and because of the timing precision of the lidar system. Figure 22 shows these data in a plot for a segment of the flight on 14 July 1990, when the lidar was in operation. The small "bumps" on the curve reflect the times when the aircraft was banking. This artifact is introduced into the plot because the simple algorithm that calculated aircraft height from the lidar return did not compensate for the bank angle of aircraft. Three levels of flights were flown in this time segment.

Figure 23 shows the calculated optical depth from aureole information over the same span of time as that of figure 22. Note that the shaded area represents periods when the returns were from clouds. These regions are tagged because there was a high probability of multiple scattering taking place here and, therefore, the single-scattering assumption and the related optical-depth calculations for these regions were not correct. Also note that although the altitude of the aircraft changed significantly over this segment of time, these variations did not noticeably affect the net optical depth, indicating that most of the optical depth was in the lowest layers of the atmosphere. While the variation in the optical depth from point to point was probably noise, the slower variation was most likely generated by slow changes in the boundary layer under the flight path.

Figures 24a and 24b contain plots of extinction as a function of altitude using the algorithm discussed above. Figure 24a shows a sequence of lidar shots taken about three seconds apart at a location of 24.10° north and 80.58° west. The results show that the variations between the individual profiles were small. They also show a well-defined boundary layer (indicated by an almost constant extinction value extending to about 450 meters in altitude in the well-mixed area just above the sea surface.) Just above this level is a zone of about 50 meters of an interfacial transition above the boundary layer in the altitude range of about 450 to 500 m. In figure 24b, we see a similar series of extinction profiles calculated with the lidar signals over a 15-second period. Here a marked change in the boundary layer is noted: it increased from 450 m to somewhere from 550 to 750 m. It is also important to note that this apparent change caused an amount of uncertainty in the extinction profile and the associated optical depth of the column.

An estimate of the boundary-layer height can be obtained by determining the altitude where the semiconstant extinction at the surface suddenly starts to drop off with altitude. Figure 25 shows a plot of the boundary-layer height as a function of flight time on 14 July. The height of the cloud top is plotted for those times when the lidar was looking down through a cloudy layer. Typically, the boundary-layer was 400 to 500 m deep. These measurements and the independent measurements made by TNO (figure 21) agree well. While the boundary-layer structure could be discerned down to a 7.5-m resolution, the interfacial zone was approximately 50 m deep and creates an uncertainty in determining the actual boundary-layer depth. This is the result of not having a strong capping inversion (such as the one that exists much of the time off of the California coast), creating a very stable boundary layer that is easy to determine.

In figure 26, the time history of the surface extinction (at a 15-m altitude) is plotted. The values have an error that is probably greater than 20%, even though they were averaged over one minute. The point-to-point variation was probably caused by noise, while long term variations may represent changes in aerosol extinction.

The aureole and lidar data were analyzed to provide estimates of the optical depth, boundary depth, and extinction profiles under the aircraft flight path. The aircraft data were also analyzed to determine the aircraft location for each stored profile. Calculating the aircraft track combined direct observations of the aircraft position at approximately 10-minute intervals with aircraft speed, direction, and times of aircraft turns. The resulting aircraft positions had an error of approximately 3 nm.

COMMENTS ON THE LIDAR MEASUREMENTS

The backscatter profiles measured with the TNO mini lidar compare favorably with both the shapes of the extinction profiles and the boundary-layer structure measured by the NRL airborne lidar system. The mixed-layer height was observed at similar altitudes and both systems mapped convective plumes. The ratio between the TNO backscatter and the NRL extinction coefficients is about 0.1, which agrees with earlier measurements of backscatter and extinction ratios. A direct comparison between the results obtained with the two lidar systems is not feasible because of the horizontal separation. Due to the geometric attenuation of lidar, the airborne system is in a better position to detect the low aerosol concentrations above the boundary layer than the land-based system. In the boundary layer, however, similar results were obtained. The advantage of the ground-based system is that it is more cost-effective for measurements of the temporal variability during extended periods.

DISCUSSION

For each day of the KEY-90 experiment, sufficient data were available to prepare both a surface observation file and a meteorological profile file. These two files are required to run NOVAM and, once they are determined, NOVAM can be used to calculate the profile of extinction at any wavelength within its range. As discussed above, the two input data files were obtained from a detailed statistical analysis of all the data sources available.

The surface observation files for the entire experiment are found in table form in the appendix of this report. The numbers in these tables characterize the best representative values of these parameters for the time periods when the boat was at the rendezvous point.

Several sets of meteorological profile data are available for each of the observation days. Those profiles obtained in the vicinity of the boat and during the time of the rendezvous were given preference over those taken at slightly different times or places. However, the general shape and significant features of the curves did not change appreciably for any of the profiles obtained during any particular experiment day, and, therefore, the results of the NOVAM calculation would not change appreciably when either one or the other was used.

The concept of temperature inversion refers to the inversion of the temperature gradient in the atmosphere. The air temperature generally gets lower with increasing height, but occasionally, especially at the top of the marine boundary layer, the reverse is the case. Inversions are very common over the waters along the west coast of California. When the air temperature starts to increase with increasing height, an inversion is said to exist. The existence of one or two inversions in the marine atmosphere, the heights and the extent over which they occur, and the magnitude of temperature change at the inversion are information that NOVAM uses to predict the aerosol concentration profile existing in the atmosphere.

Each experiment day's profiles were examined and analyzed for the existence and location of inversions if any. The experimental conditions during KEY-90 were very different from those of the FIRE experiment, because all KEY-90 profiles showed no real temperature inversion within the range of altitudes over which the profile data were taken. Data from the FIRE experiment, on the other hand, had a majority of the cases with one or two strong temperature inversions. This was one of the major differences expected between the west coast region, as represented by the FIRE experiment, and the "tropical" region, as represented by the KEY-90 experiment.

An appreciable amount of data was taken during this experiment. Unfortunately, because of space limitations, only a small amount of the total data is reproduced in usable form in this report. Some parts of the experimental data taken from KEY-90 are used in only the statistical analysis and cannot be recovered from the text for other uses and applications. The reader should contact one of the individual authors of this report if interested in more details of those types of data.

14 JULY DATA ANALYSIS IN THE VERIFICATION OF NOVAM

The verification process starts with determining the surface observation file for the period in question. The values of the NOVAM parameters needed in the 14 July 1990 surface observation file are found in table 12.

Table 12. Surface observation file for 14 July 1990.

Parameter	Value
Sea Surface Temperature (C)	29.7
Air Temperature (C)	28.2
Relative Humidity (%)	82.6
Optical Visibility (km)	26
Current Real Wind Speed (m/s)	5.4
Average Wind Speed [24 Hours] (m/s)	5.1
Air Mass Parameter [1..30]	1.6
Cloud Cover (tenths)	0.3
Cloud Type [0..10]	8
Surface IR Ext. (1/km) @ 10.6 μ	0.444
Present Weather in Standard Code [0–99]	3
Height of Lowest Cloud (m)	250
Zonal/Season Category (1.6)	2

The KEY-90 group performed six meteorological soundings during 14 July. Of these, one aircraft sounding was done close to the boat while at the rendezvous point. Radiosonde number 8 (figure 27) was also made at the boat during the rendezvous, and number 9 was obtained back in Marathon at the boat dock later in the day. The other aircraft soundings were done farther away from the site in conjunction with simultaneous aerosol extinction measurements with the airborne lidar at different locations.

Figure 28 shows the plot of air temperature profiles obtained from the NOSC aircraft and the two radiosondes shown in figure 27 for 14 July 1990. Although the potential temperature profiles of

figure 27 indicate some sort of free mixing zone below 500 m, the air temperature profile showed that this region was not capped by a temperature inversion. Since there were no temperature inversions in the air temperature profiles, the simple case of no inversions was used to run the NOVAM. The preamble to the file used to indicate this fact is shown in table 13. In this table, only the first row of data describes actual data from the profile. The numbers in the first row are the following: (1) the number of observations in the meteorological profile file, (2) the potential temperature at the lowest level, and (3) the mixing ratio at the lowest level. The other 12 numbers are ignored by NOVAM in this case. The "-999" is the key by which the no-inversion situation is indicated to the model (Gathman, 1989).

Table 13. Preamble to the meteorological profile data file for 14 July 1990.

174	28.1	18.7
-999	-999	-999
1	-999	-999
-999	-999	-999
1	-999	-999

Once the input files are available, NOVAM can be run to determine the extinction profile, and the extinction profile's results can be plotted together with the other types of measured extinction. Such a plot is seen in figure 29, where the NOVAM-predicted extinction profile for 1.06 μ is shown by the thick solid line. Plotted in the graph are other extinction measurements made at the same wavelength obtained from Mie calculations on the aerosol size distribution measured simultaneously by the NOSC aircraft with the profile data used in NOVAM. In addition, an extinction profile deduced from the downward-looking aureole lidar at a nearby location is shown. Also in the plot is the extinction value at the surface for that same wavelength obtained from Mie calculations made from a long-term (1 hour) average of the size distribution made from the boat's aerosol measurement system.

Although the locations of these observations were within a few km of each other, the time scales of the data on which they were based differed quite widely from one another. First of all, the lidar return was done in a single shot of the lidar, with a time scale of the speed of light. The time required for the aerosol sampling aircraft to make the ascent from the surface to 3000 m was on the order of 20 minutes and, of course, different parts of the profile were measured in different parts of the atmosphere as the aircraft circled. The surface aerosol size distribution is considered the most reliable in terms of a long-term average, since it was obtained by averaging particle data for a period of greater than an hour. The NOVAM plot used information from the surface as well as from the best of the meteorological profile made from the aircraft sounding. The plot must, therefore, be thought of as an average profile that would exist at the rendezvous point.

One odd feature of the aircraft aerosol profile is the apparent dropoff of extinction near the surface. Most of the aircraft profiles made during the experiment showed some tendency for this characteristic. Relative humidity perturbations in the marine boundary layer (which could cause changes in the aerosol size distribution and, hence, changes in the extinction profile) do not indicate that particle growth is the reason for this behavior. In order to investigate this phenomenon, the aerosol size distribution was looked at in more detail.

Because this was a meteorologically convective environment, convective cells were close to the sea surface. This cellular structure was detected by both lidars, which showed that aerosol scattering in this region was not uniform in the horizontal direction but that the returns could be interpreted to be produced by different aerosol-laden air parcels flowing either upward or downward in convective

columns. We cannot answer the question of what percentage of time the aircraft was in a downward-flowing column of air while the aircraft was flying in a spiral pattern. Flight patterns that spent too much time in one or the other of the flow cells might show a distorted size distribution because of the flow of aerosol in the cellular motion. In addition, there has to be a compromise between the length of time spent at each altitude (in order to obtain enough aerosol particles to statistically give a reasonable value) and the number of levels to sample within the time available for the profile and consistent with the horizontal homogeneity assumption.

Figure 30 shows the aerosol size distribution near the sea surface. This aerosol size distribution was obtained from three sets of real data as well as from the NOVAM-determined size distribution. In this figure, we are looking only at levels close to the sea surface and thus the vertical structure of the NOVAM model is not tested. Here we see that the size distribution at the bottom of the aircraft extinction profile (solid heavy line) did not see any particles larger than a 1-μ radius. Also available at a time and place adjacent to where the profile data was taken is a run of 10 miles of level flight where extinction averages were determined near the sea's surface (circles). This shows that particles out to a 10-μ radius were observed by the aircraft if sufficient time was available for the measurement, and these data agree well with the boat values, which are averages obtained over about 1 hour. Model results (thin solid line) show a slight overestimation in dN/dr at radii below about 2 or 3 μ radius and an underestimation at radii larger than these values.

There are large variations between adjacent short-term average measurements in the aircraft extinction data. In addition, the two-dimensional maps of aerosol scatter made by both of the lidars indicate a cell-like structure near the sea surface. These facts indicate that the usual horizontal homogeneity assumption is not too well founded in this region. This causes a problem in the verification of NOVAM, which is a "time averaged" model giving an average extinction profile from average meteorological profile inputs. What is needed is a time–average measured extinction profile to which NOVAM's prediction can be compared. The best we can do is to "smooth" the aircraft-derived profiles.

The aircraft measurement sampling time at each level of the profile was, by necessity, short, compared with the surface boat's "long averaging time" of an hour, which was needed for the verification of NOVAM. This means that the standard by which we are to judge the performance of the NOVAM model will be a "smoothed" profile containing a fair amount of uncertainty.

The extinction data at any wavelength could be obtained from the aircraft aerosol measurements. To see how the long wave data look, the 10.6-μm extinction values from the flight are plotted as circles in figure 31. From these data, maximum and minimum curves, which depicted the spread in the data in a reproducible way, were developed. These curves were derived by the following method: the extinction data were converted to logarithms to the base 10 and a smoothed version of the extinction profile was fitted to the data points by using the polynomial regression method of the sixth order. From this curve, the differences between the data points and the smoothed curve were extracted. The rms of these differences as a function of altitude was determined. These data were also smoothed by means of a sixth-order polynomial. The maximum part of the envelope profile was calculated by adding twice the smoothed rms of the differences to the smoothed extinction profile. Likewise, the minimum part of the envelope profile was calculated by subtracting twice the smoothed rms of the differences from the smoothed extinction profile.

One measure of the success of the experiment, then, could be based on whether or not the NOVAM-determined profile was as good as that of the measurements. That is, do the NOVAM values fall within the envelope of the measured data? Given that we have now defined a maximum and minimum of the data envelope, the criterion is if the values from the model fall within the limits of the envelope.

Using this criterion, the model was graded for all the experiments in KEY-90. The grading for each case then depended on where the NOVAM value was at each level with respect to the data envelope and the 2x data envelope. Clearly, if the model were always contained within the data envelope, then it would be working as well as could be ascertained from the data measurements, and we would give this a grade of "A." The other grades are shown in the grading key box in figure 32. The pie charts here seem to indicate that the model gets better at the longer wavelengths. Unfortunately, this is not really the case.

The problem with this system of grading is that as the variance in the measurement decreases, the grades also tend to decrease. Clearly, if a measurement gave a very thin line that had no variance, then the possibility of exactly matching these data with a model prediction would indeed be small. This process is shown in the figure where NOVAM's grades progress to better and better values as the wavelength goes from visible to the far infrared. This is probably caused by sampling error problems. In the atmosphere in the regions of radii larger than 0.05 μ, the aerosol concentration generally decreases as the size of the aerosol radius increases. For a finite sampling time, this causes the variance in the extinction data derived from measured aerosol to become larger at the longer wavelengths.

The problem in evaluating the performance of a model like NOVAM is finding a suitable standard by which to judge the result. The object being judged by a standard can only be as good as the standard by which it is judged. It might represent the true situation more precisely that does the standard but since there is nothing else by which to judge it, the uncertainty of the standard must also be applied to the model even if all of the data fits within the envelope.

In KEY-90, the meteorology of each experiment day was more or less similar. Consequently, only one type of atmospheric model was detected and used by NOVAM, and a more statistical approach could be made in comparing model with measurement. Figure 33 plots of all the 3.5-μ extinction measurements from the aircraft profiles from the KEY-90 experiment together. This plot shows that although there was a large scatter in individual points, the points tend to cluster about a profile that could be represented by a segmented straight line on the log-linear plot. The lower drop-off of extinction between 400 m and the ocean surface shows up on the plot, but this feature will be ignored because of the explanation given above. A linear least squares fit was made of all of these data (including that of the drop off at the surface) and is shown by the labeled line in the figure. From similar data obtained with NOVAM for all these cases, a similar least squares fit of predicted values was made to a line, and it is shown plotted on the same curve as the measurements. It is seen that the agreement between model and measurement, when averaged over a large amount of data, was reasonable and encouraging. Perhaps the model's scale heights of the extinction profiles should, in this case, be adjusted by a small amount to minimize even this difference. The data in figure 33 show that the extinction at any particular time and place may be very different another time, even though the atmospheric conditions are quite similar.

In table 14, we see a portion of the statistics obtained in the regression analysis that was used in determining the least squares fit of both the aircraft data and the NOVAM-predicted data. The table shows some of the analysis of the variance statistics from this study. The table shows the mean square of the data as it spreads out from the regression line. The units of measurement here are logs of extinction, so the spread in the data is directly represented in the log-linear plot of figure 33, where the value of 1 refers to an order of magnitude in the mean square of the residual of the regression. A distinct increase in the mean square of the data from the aircraft as the wavelength increases is seen in the table. This is the result of the lack of aerosols available for the measurement at the larger aerosol sizes, which are needed for the Mie calculation at the longer wavelengths. This is the cause of the apparent increase in grades shown in figure 32.

Table 14. A portion of the statistics obtained in the regression analysis.

Wavelength (μ)	Mean square of aircraft measurements [log of ext.]	Mean square of NOVAM data [log of ext.]
0.55	1.612	0.450
1.06	1.966	0.406
3.5	3.706	0.401
10.6	3.983	0.477

The same set of statistical data used in the regression study shows that the slope of the regression line for the NOVAM data test differs from the regression line slope of the aircraft data by about 20% over all the wavelengths. The slope here is again expressed in terms of the change in altitude (m) per change in the log of extinction. In the measured data, there appears to be a slight increase in slope magnitude with increasing wavelength, indicating that the scale height of the larger particles is less than that of the smaller particles.

A third way of evaluating NOVAM with the aircraft-derived data of KEY-90 looks at a smoothed version, then compares the smoothed versions with each other. Figure 34 shows this type of comparison for the special day of 14 July 1990. The solid line in the figure represents a sixth-order polynomial fit to the aircraft measurements from that day. The actual data points of the aircraft are shown by the small open circles and are similar to those shown in figure 31. The one hour average extinction made by the boat at the surface is shown by the large black circle at the surface. From these data, it is seen that NOVAM did rather well in representing the average extinction profile for the region, but because of the "average" nature of its predictions, it did not show the peak in the measured extinction in the region of 500 to 700 m and from 1800 to 2300 m.

It is reasonable to assume that these polynomials represent an ensemble "average" profile that would exist if many determinations of the profiles were done in the same air mass at the same time. This interpretation then allows a deeper probe into the data than was possible with the overall linear regression that was used in the above analysis. In particular, the two layers shown in the "average" curve in the figure can be identified with lidar structures shown in both the shore-based and aircraft lidars (figures 19, 20, 24a and 24b), giving credence to the validity of this assumption. If this is true, then we can look at the statistics in an individual, aircraft-derived extinction profile and determine more precisely the performance of NOVAM in order to fit this particular data set. Figure 35 plots the histogram of the variance of the aircraft measurements about the smooth "average" profile, as determined by the regression fit. The data shows some observations considerably outside the normal distribution. We know from other sources that the largest observation was from the aircraft penetration of a cloud by the aircraft while it was in the process of making a complete spiral. The standard deviation of log of these variance data is 0.89. This can be converted to extinction maximum/minimum values by considering a mean extinction of 0.01 1/km. This kind of variance then gives a maximum/minimum spread of 0.077 and 0.0013 (1/km) which is just under an order of magnitude in spread. While this still seems high in value, it is much smaller than what we obtained from the overall averages for 10.6 μ in table 14.

On the other hand, if we do the same analysis on the variation of the NOVAM data from the smooth "average" plot, we get the histogram shown in figure 36. This data set has a logarithm to base of 10 variance of 0.06, which translates (for a mean value of 0.01 1/km) into a maximum/minimum envelope of 0.011 and 0.0087, which is quite sharply defined. Most of this variation comes from the fluctuations in the relative humidity measurements from the meteorological profile data file used as input to NOVAM.

Now with the assumption that the smoothed aircraft extinction profile is "truth," then we want to know how much variation exists between the average aircraft measurement and the average NOVAM calculation. By looking at 100 equally spaced levels, a histogram of these data can be obtained (figure 37). Here the variance shows a standard deviation of 0.30 for the 10.6 μ case of 14 July 1990. This translates (for the case of average ext. = 0.01) into a maximum/minimum spread of 0.02 and 0.005.

CONCLUSION

KEY-90 was a successful experiment because the major goal of the experiment (to obtain quality data to test NOVAM for every working day of the experiment in the tropical area) was met. The data set contained even more information than was needed for the testing of NOVAM, and the authors will use this data set for future publications. In addition, the data set contains sufficient information so that insight into certain mechanisms at work in this environment can be made. This paper contains some insight into the physical processes that took place for the special day of 14 July 1990. The analysis for the other days of the experiment remains to be done.

In the tropical marine environment, such as was found during the experiments of KEY-90, natural variations in the characteristics of the marine boundary layer (in both time and space) cause instantaneous and average extinction profiles to be different from each other. Statistical techniques must therefore be used to determine if the model that predicts average optical/infrared characteristics and the instantaneously measured optical/IR data are equivalent. The paper presents three approaches to this problem and shows that NOVAM did a good job predicting the extinction profile of the marine boundary layer, given only the two meteorological data files. The tests in this report describe the operation of the model when all the required data are available, but the report does not address the problem of what the performance of the model is if the required input data were inaccurate or missing.

The data from KEY-90 were very different than what was found in the FIRE experiment at San Nicholas Island off the California coast. The Florida coast contained convective clouds and warm surface water, whereas the San Nicholas weather consisted usually of stable air over cold surface waters. Unlike the FIRE experiment, the Key-90 experiment never saw a true temperature inversion measured. The experiment therefore tested only the "no inversion" case for NOVAM.

REFERENCES

Davidson, K. L., and C. W. Fairall. 1986. "Optical Properties of the Marine Atmospheric Boundary Layer: Aerosol Profiles." SPIE, vol. 637, Ocean Optics VIII.

Davidson, K. L., G. de Leeuw, S. G. Gathman, and D.R. Jensen. 1990. "Verification of the Naval Oceanic Vertical Aerosol Model During FIRE." In *FIRE Science Results* 1989, pp. 191–196, D.S. McDougal, Ed. NASA Conference Report 3079.

de Leeuw, G. 1986. "Vertical Profiles of Giant Particles Close Above the Sea Surface." *Tellus*, 38B, pp. 51–61.

de Leeuw, G., K. L .Davidson, S. G. Gathman, and V. R. Noonkester. 1989a. "Modeling of Aerosols in the Marine Mixed-Layer." SPIE Vol: 1115, *Propagation Engineering*, p 287–294.

de Leeuw, G., K. L. Davidson, S. G. Gathman, and V. R. Noonkester. 1989b. "Physical Models for Aerosol in the Marine Mixed Layer." paper 40 at AGARD conference proceeding #453 on *Operational Decision Aids For Exploiting Or Mitigating Electromagnetic Propagation Effects*, AGARD–CP–453, Electromagnetic Wave Propagation Panel Symposium, San Diego, CA. 15–19 May 1989.

de Leeuw, G. 1990. "Profiling of Aerosol Concentrations, Particle Size Distributions, and Relative Humidity in the Atmospheric Surface Layer over the North Sea." *Tellus 42B* (1990), 4, pp. 342–354.

de Leeuw, G., G. J. Kunz, and M. M. Moerman. 1991. "Lidar and Aerosol Measurements by the TNO Physics and Electronics Laboratory during KEY-90 (Marathon, FL, USA; 2–19 July, 1990)." TNO Physics and Electronics Laboratory, PO Box 96864, the Hague, the Netherlands.

Fairall, C. W., and K. L. Davidson. 1986. "Dynamics and Modeling of Aerosols in the Marine Atmospheric Boundary Layer." In *Oceanic Whitecaps and their Role in Air–Sea Exchange Processes*, pp. 195–20, E.C.Monahan & G.MacNiocaill Eds. D. Reidel Publishing Co., *Dordrecht*.

Gathman, S. G. 1978. "Model for Estimating Meteorological Profiles from Shipboard Observations," NRL Rpt. 8279.

Gathman, S. 1983a. "Optical Properties of the Marine Aerosol as predicted by the Navy Aerosol Model", *Optical Engineering*, vol. 22, no. 1, pp. 57–62.

Gathman, S. G. 1983b. "Optical Properties of the Marine Aerosol as Predicted by a BASIC Version of the Navy Aerosol Model", *NRL memo rept 5157*.

Gathman, S. G. 1984. "Navy Hygroscopic Aerosol Model." In *Hygroscopic Aerosol*, p. 93, L.H. Ruhnke & A. Deepak, Eds. A. Deepak Hampton, VA.

Gathman, S. G. 1989. "A Preliminary Description of NOVAM, the Navy Oceanic Vertical Aerosol Model," NRL report 9200.

Gathman, S. G., G. deLeeuw, K. L. Davidson, and D. R. Jensen. 1990. "The Navy Oceanic Vertical Aerosol Model: Progress Report." AGARD, 45th Symposium, Electromagnetic Wave Propagation Panel on Atmospheric Propagation , Copenhagen, Denmark, 9–11 Oct 1989, c.p.454, no. 17

Gerber, H. 1989. "Measurement of Suspended Particulate Volume and Far-Infrared Extinction Coefficient with a New Laser-Diffraction Instrument." European Aerosol Conference, Wien.

Gerber, H. 1991. "Direct Measurement of Suspended Particulate Volume Concentration and Far-Infared Extinction Coefficient with a Laser Diffraction Instrument," *Applied Optics*, vol. 33, pp. 4824–4831.

Gerber, H., S. Gathman, J. James, M. Smith, I. Consterdine, and S. Brandeki. 1990. "NRL Tethered Balloon Measurements at San Nicolas Island During FIRE IFO 1987." In *FIRE Science Results 1988*, pp. 191–196, D. S. McDougal and H. S. Wagner, Eds. NASA conference publication no. 3079.

Hooper, W. P. and H. E. Gerber. 1986. "Down Looking Lidar Inversion Constrained by Ocean Reflection and Forward Scatter of Laser Light," *Applied Optics*, vol. 25, p. 689.

Hooper, W. P. and H. Gerber. 1988. "Monte Carlo Simulations of Laser-Generated Sea Surface Aureole," *Applied Optics*, vol. 27, p. 5111.

Hooper, W. P. and E. W. Eloranta. 1986. "Lidar Measurements of Wind in the Planetary Boundar Layer: the Method, accuracy and Results from Joint Measurements with Radiosonde and Kytoon," *JCAM* vol. 25, no. 7, p. 990.

Hughes, H. G. 1987. "Evaluation of the Lowtran 6 Navy Maritime Aerosol Model Using 8 to 12 Micron Sky Radiances," *Optics Engineering*, vol. 26, no.. 11, p. 1155.

Jensen, D. R. 1978. "Aerosol Measurements in the Marine Boundary Layer at San Diego," NOSC TR 168, Naval Ocean Systems Center, San Diego, CA.

Kneizys, F.X., E. P. Shettle, W. O. Gallery, J. H. Chetwynd, Jr., L. W. Abrew, J. E. A. Selby, S. A. Clough, and R. W. Fenn. 1983. "Atmospheric Transmittance/Radiance: Computer Code LOWTRAN 6," AFGL-TR-83-0187 environmental research papers, # 846. AFGL, Hanscom Air Force Base, MA.

Winkler, P., and C. Junge. 1972. "The Growth of Atmospheric Aerosol Particles as a Function of the Relative Humidity," *Journal de recherches atmospheriques*, pp. 617–638.

ACRONYMS

cc	cloud cover
CN	condensation nuclei
ct	cloud type
EM/EO	Electromagnetic/Electro-Optical
FEL	Physics and Electronics Laboratory (taken from the Dutch)
FIRE	First ISCCP Regional Experiment
IR	infrared
IRAAMP	Infrared Analysis Measurement and Modeling Program
ISCCP	International Satellites Cloud Climatology Program
MABL	Marine Atomosphere Boundary Layer
MBL	Marine Boundary Layer
m/s	meters per second
NAM	Navy Aerosol Mold
NOVAM	Naval Oceanic Vertical Aerosol Model
NRL	Naval Research Laboratory
NPS	Naval Postgraduate School
PI	Principal Investigator
PMS	Partical Measurement System
pw	present weather
PVM	Particle Volume Meter
rms	root mean square
SST	Sea Surface Temperature
TAIR	Air Temperature
UMIST	University of Manchester Institute of Science Technology
WS	Windspeed (Data)
wx	weather observations
zcld	lowest cloud level

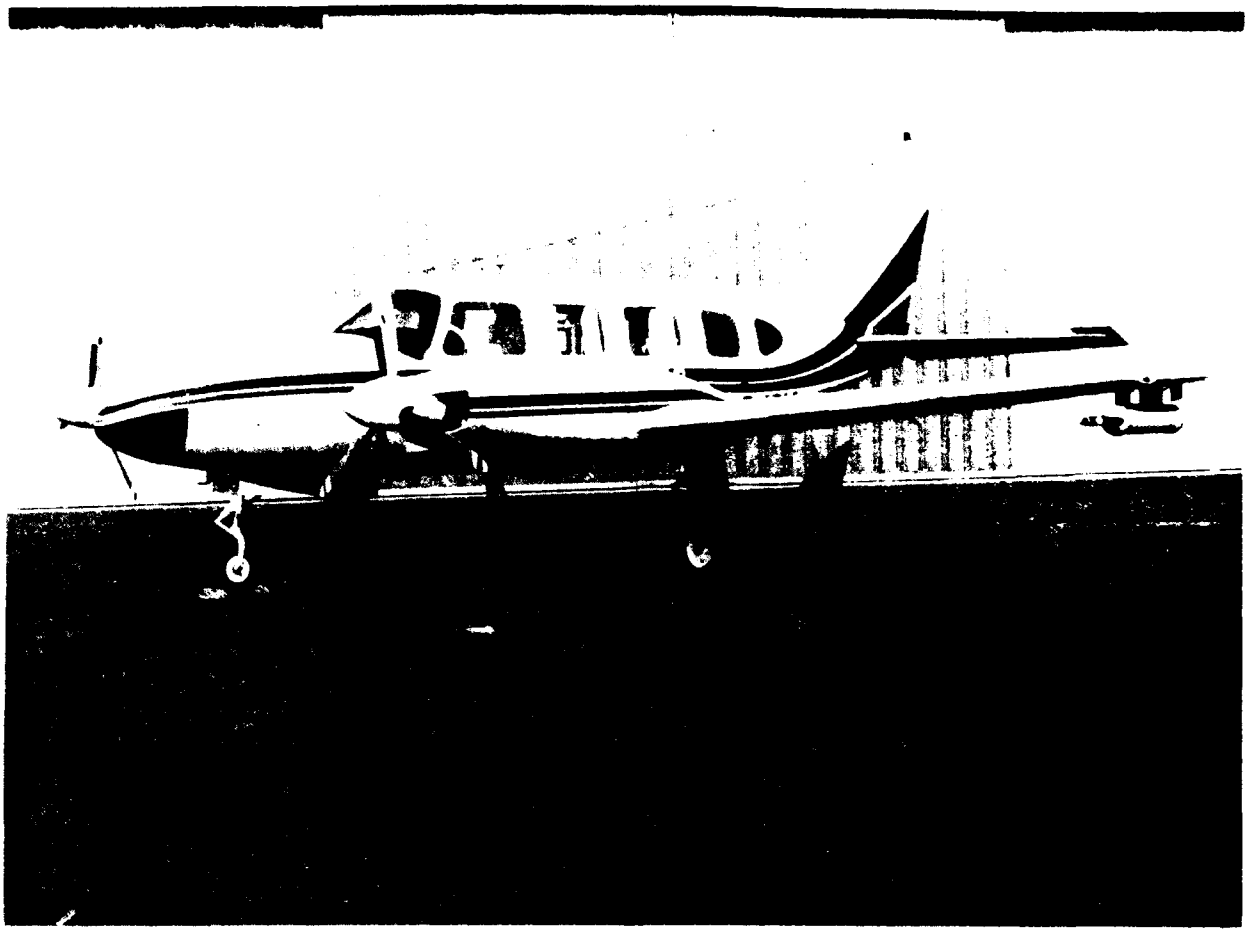

Figure 2. NOSC Navajo aircraft used in KEY-90 to make profiles of both meterological data and aerosol size distributions.

Figure 3. TNO Mini lidar as mounted during the KEY-90 experiments at the eighth floor of an apartment building in Marathon. Pointing direction is upward over ocean.

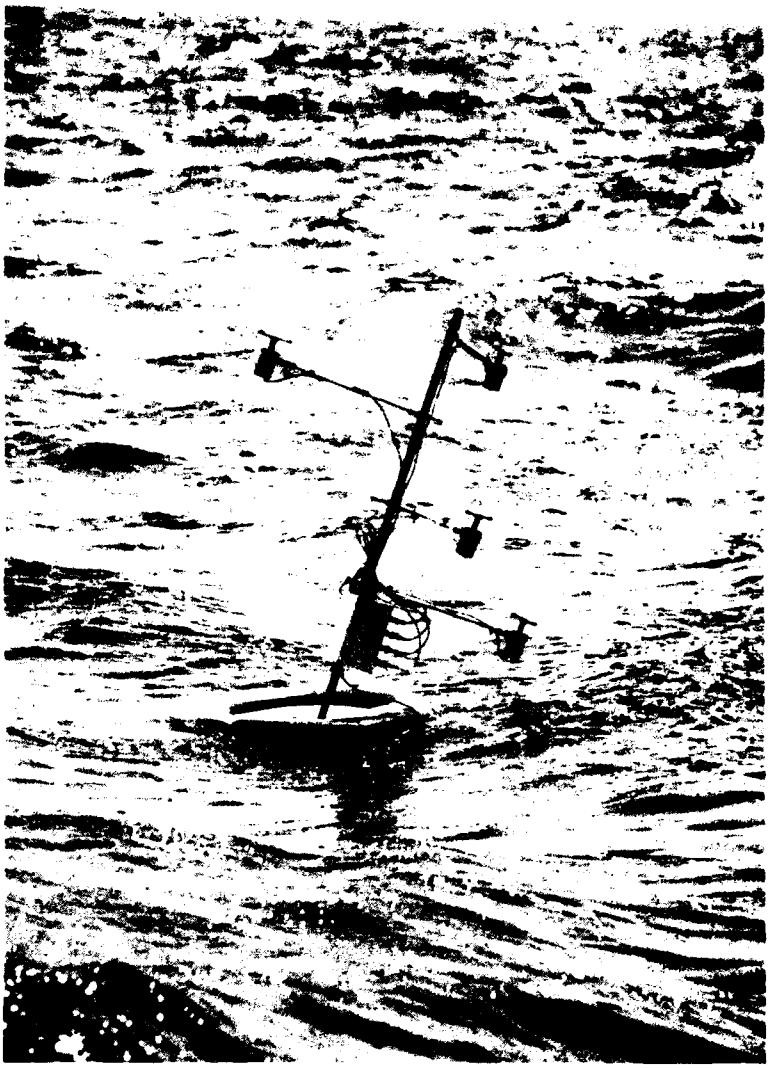

Figure 4. Wave follower with Rotorods, used for profiling particle size distributions (D>13 μm) between 0.5 and 1.25 m above the air–sea interface.

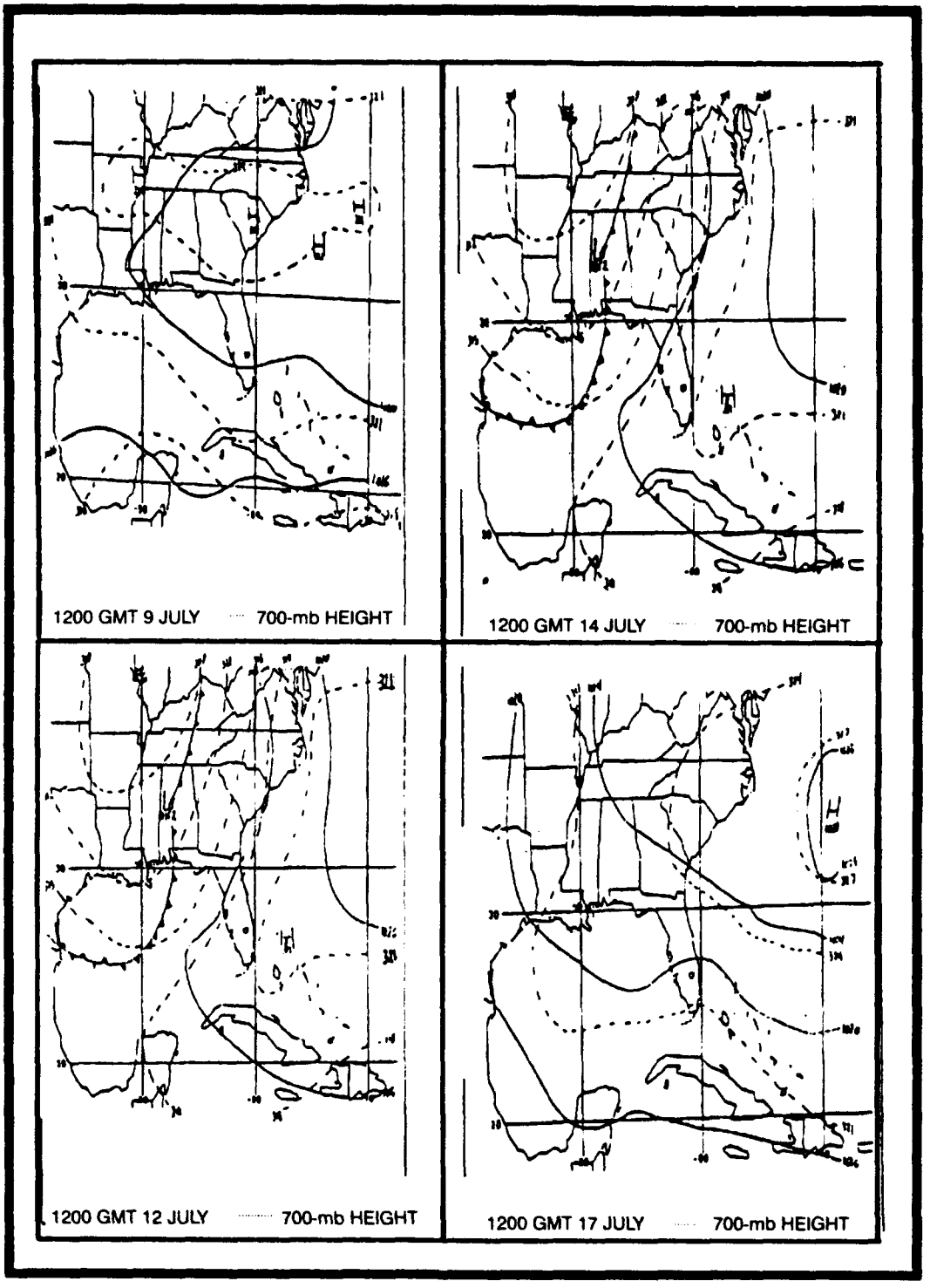

Figure 5. Synoptic weather patterns in the Marathon area: surface pressure (mb) adn 700-mb heights (m/10) from NMC analysis for 1200 GMT for 9, 12, 14, and 17 July 1990.

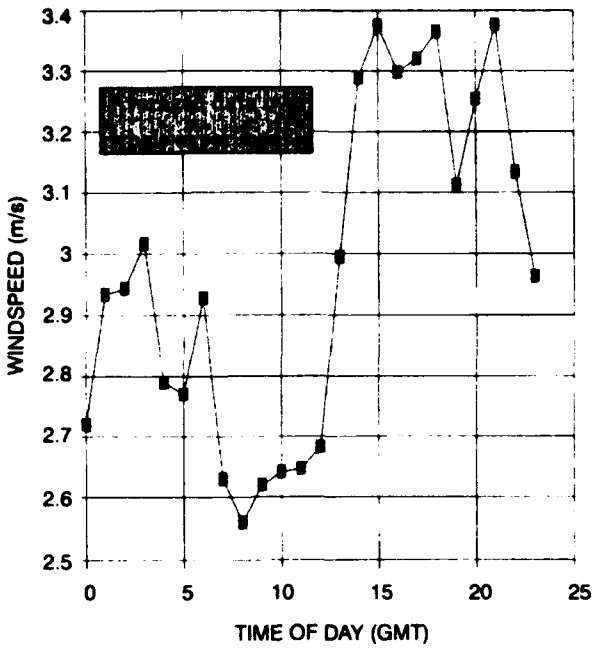

Figure 6. A plot of windspeed plotted at the airport in terms of universal time and showing the diurnal sea-breeze effect in operation on the island during KEY-90.

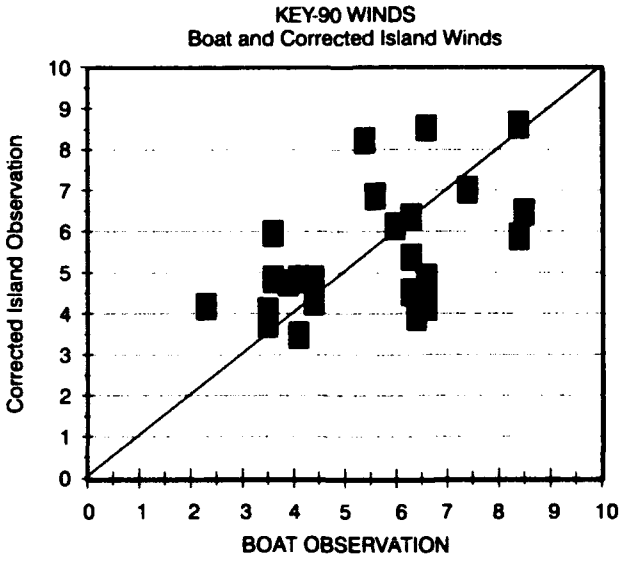

Figure 7. Scatter plot showing the wind measured at the boat compared with the "corrected" wind from the airport instrument. The correction was for both diurnal and other effects. Data covers the whole period of KEY-90 and each "observation symbol" is the time average of the wind during which the boat was stopped on the station.

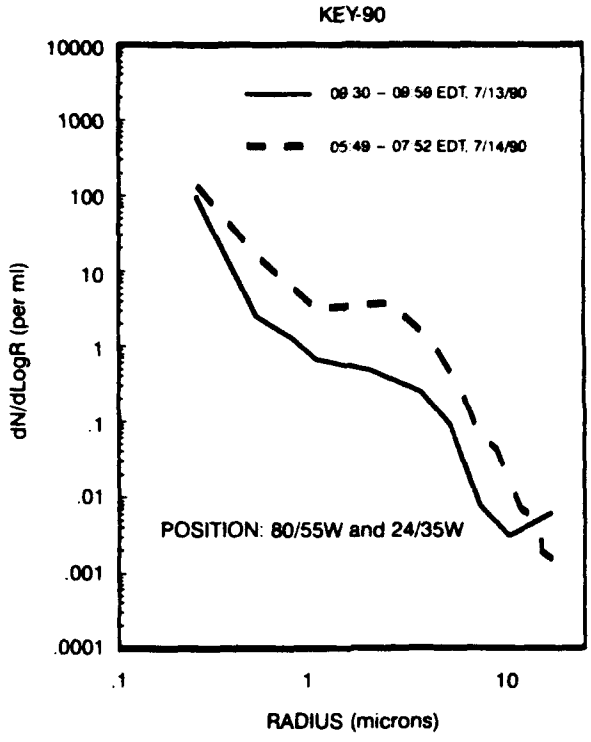

Figure 8. UMIST aerosol size distributions from the *Renegade*.

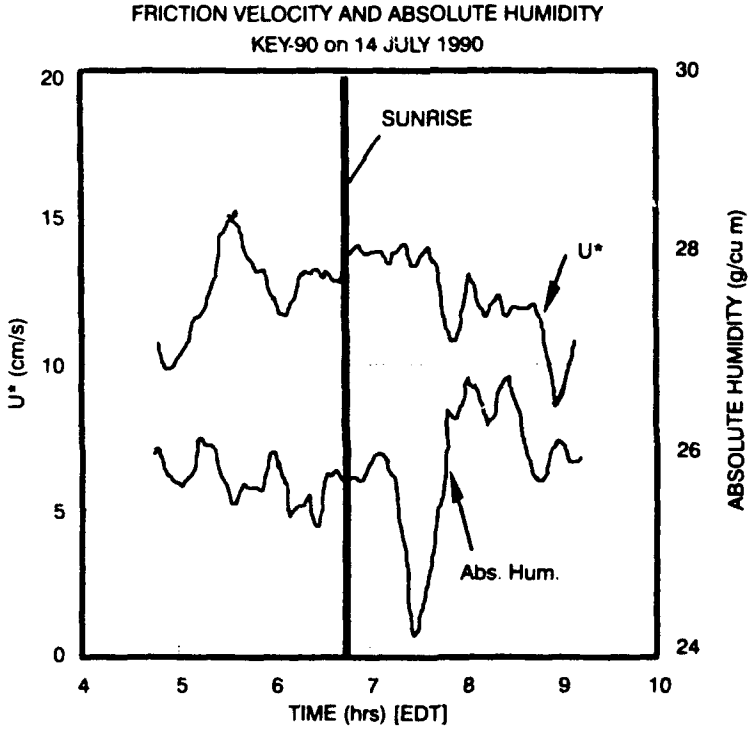

Figure 9. Variations of U* and absolute humidity during the events of 14 July 1990.

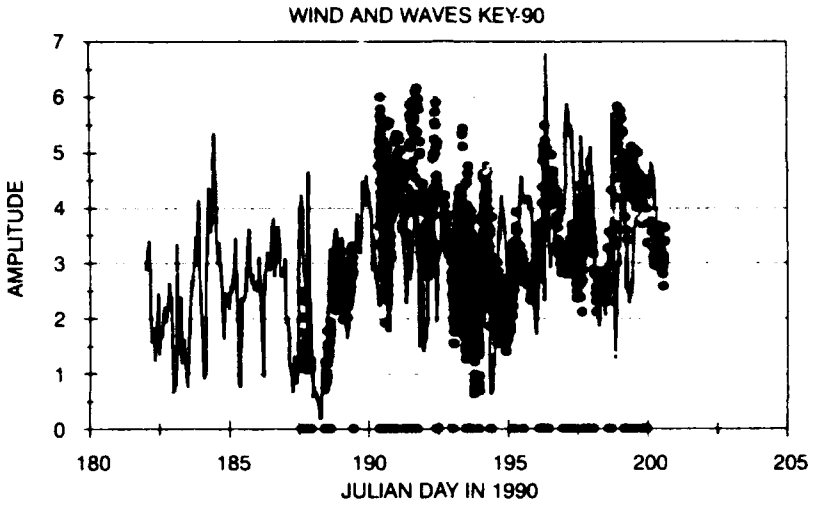

Figure 10. Plot of the windspeed and wave amplitude as a function of time during the KEY-90 experiment. In this plot, the uncorrected windspeed on the island is drawn as a solid line and the rms value of the waves from the two buoys are plotted as small circles. The numbers on the Y axis represent m per second for the windspeed measurements and 20 times the rms value of the wave height in m.

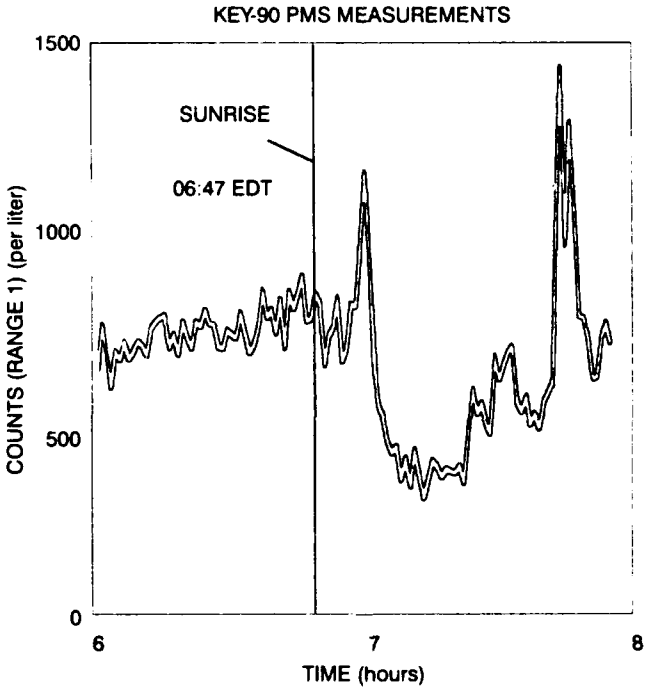

Figure 11. Temporal plot of UMIST aerosol concentration in a single channel during KEY-90 experiment on 14 July 1990.

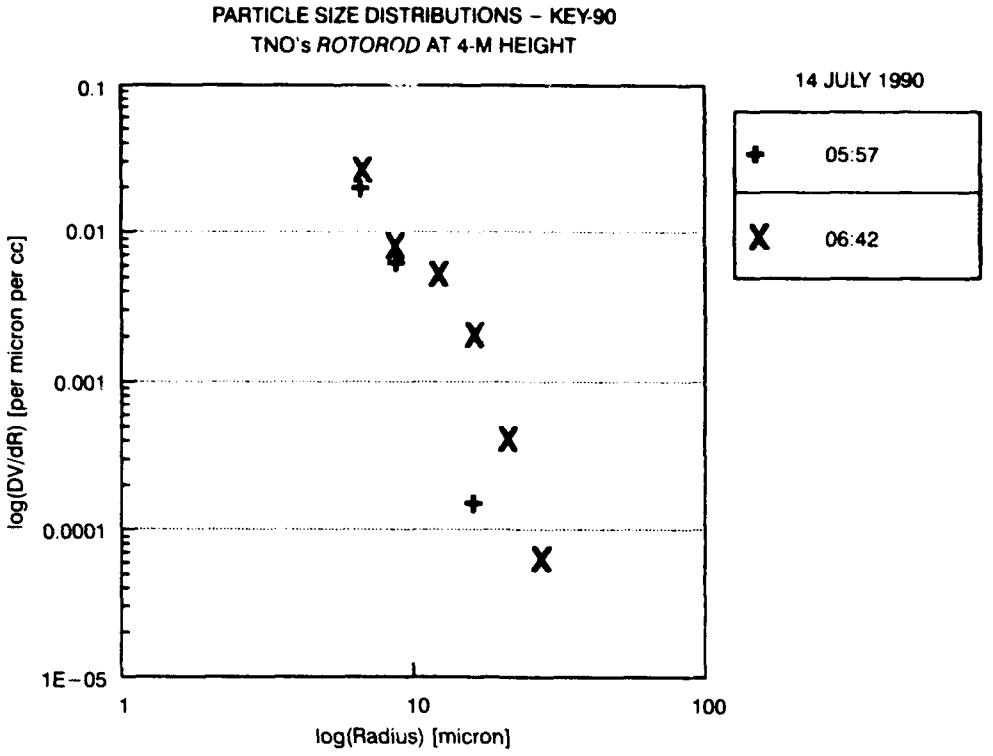

Figure 12. Particle size distributions measured from the deck of the *Renegade* at 4 m above mean sea level.

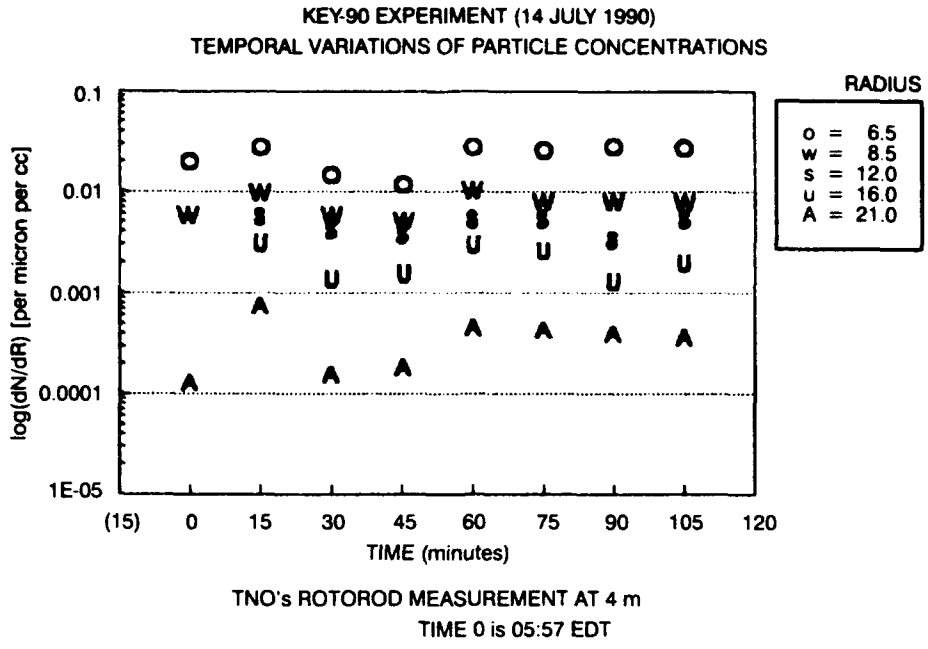

Figure 13. Temporal variations of particle concentrations during 14 July 1990 at 4 m. Data are taken from the *Renegade* while on station.

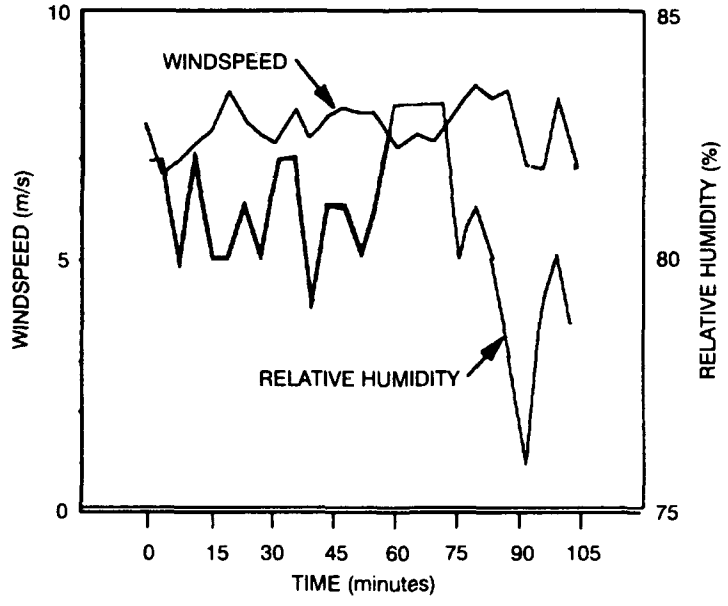

Figure 14. Relative humidity and windspeed data where time 0 is 05:57 EDT on 14 July 1990 while the *Renegade* was on station.

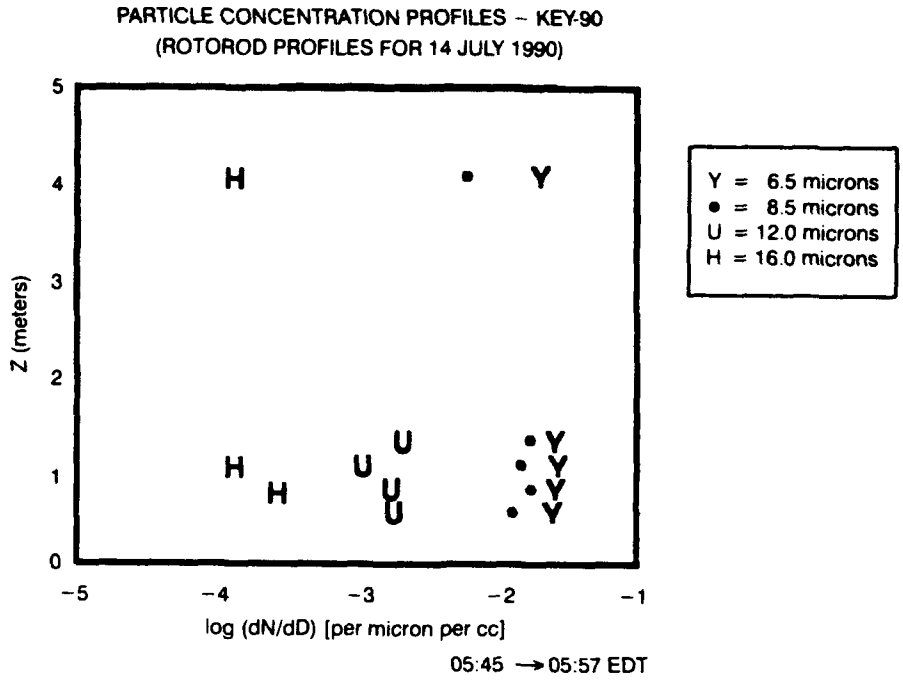

Figure 15. Concentration profiles at the lower four levels were measured from buoy and 4 m from boat.

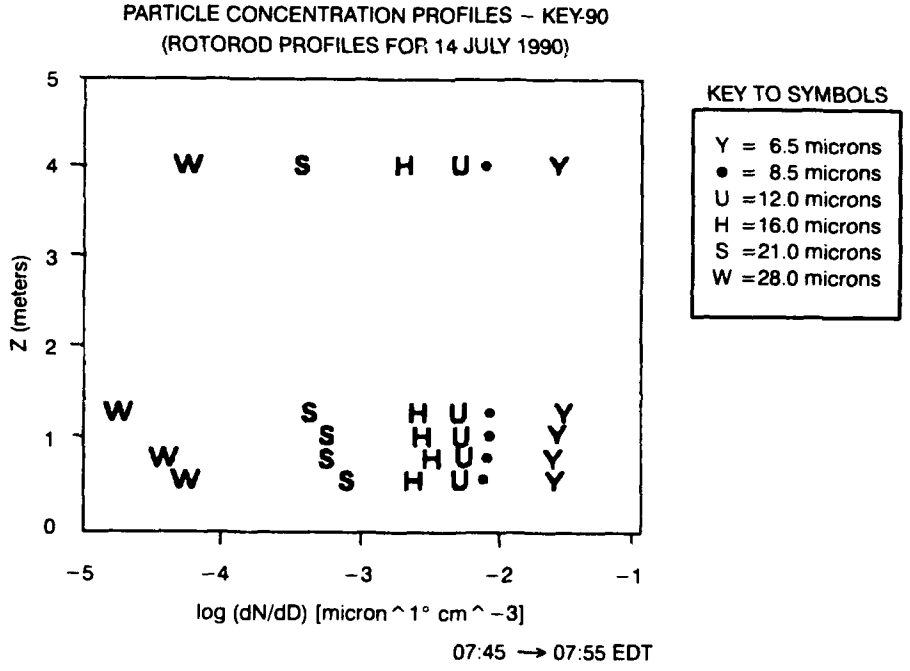

Figure 16. As in figure 15: Note statistical errors for 28-mm particles because of low counts.

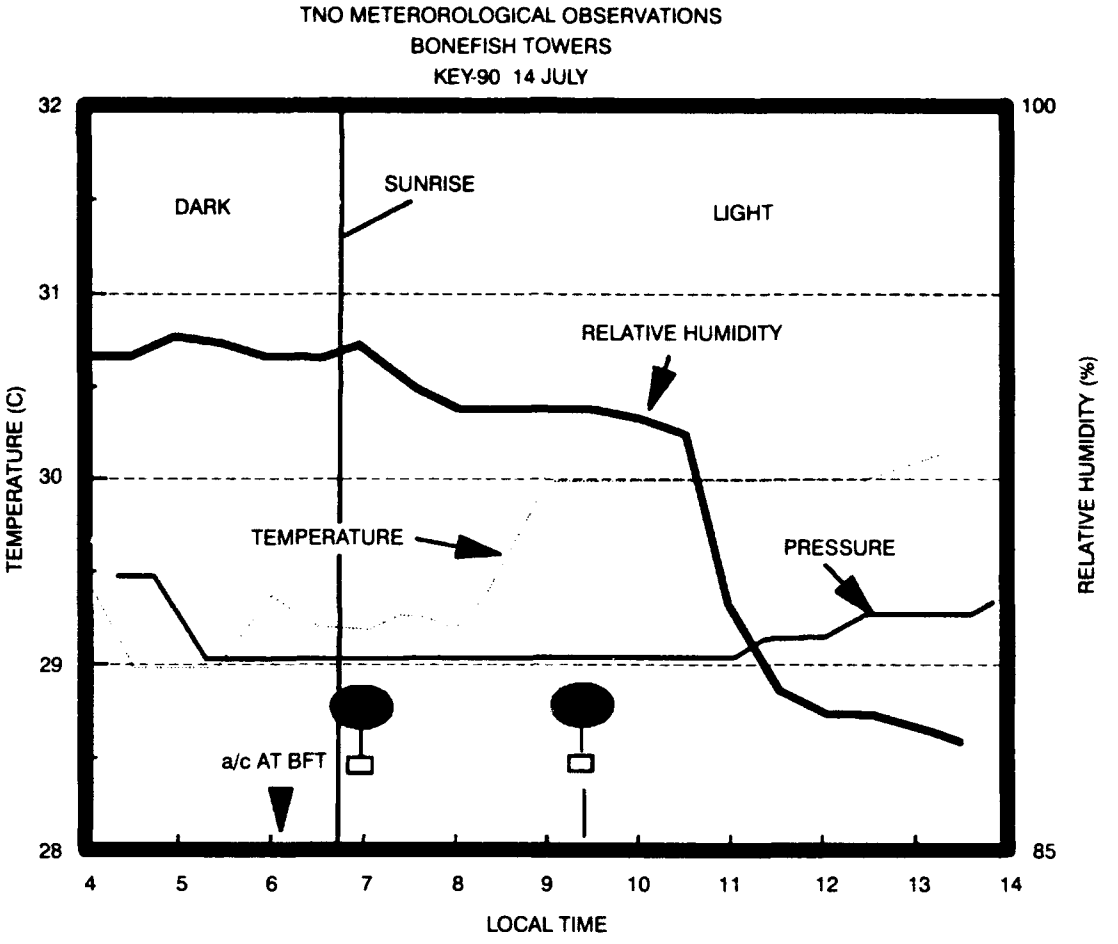

Figure 17. Temperature (dotted line), relative humidity (heavy line), and atmospheric pressure (thin solid line) as recorded at Bonefish Towers, 25 m above sea level, from 04:00 to 14:00 on 14 July. The airplane passage, as well as radiosonde launches, are indicated. The pressure scale is from 1018.5 to 1020 mb. The figure shows some temperature fluctuations during the first four hours, with a rather sharp rise of about 1°C between 0815 and 0900. The relative humidity fluctuated slightly around a value of 95% before sunrise, then dropped by about 1%. Note the sudden drop in relative humidity that occurred within 1 hour beginning at 1030 to below 88%. From this time to 1400, the relative humidity decreases slightly to 87%. The time delay between the temperature jump of 1°C and the drop in relative humidity of 8% was about 2 hours.

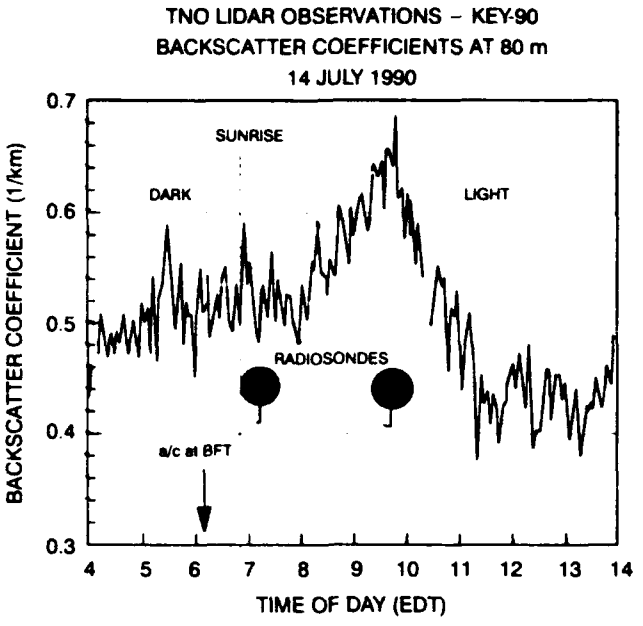

Figure 18. Backscatter coefficients in 1/km at an altitude of 80 m, from 04:00 to 14:00, averaged over 2-minute intervals.

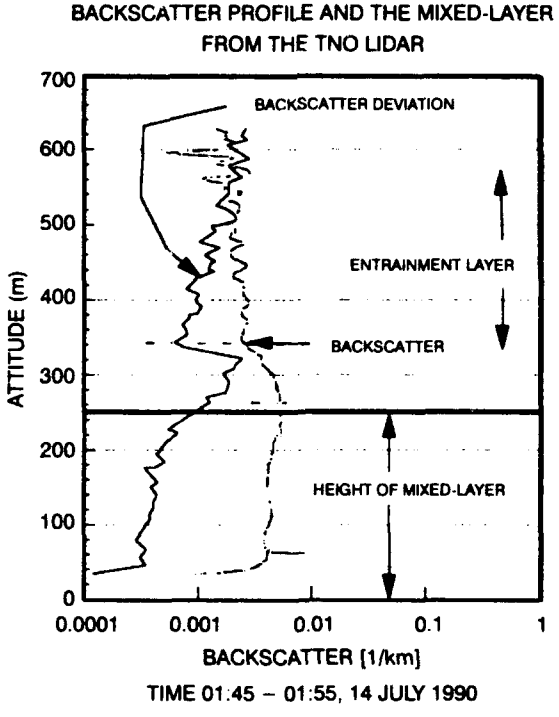

Figure 19. Profiles of backscatter coefficients averaged over 10 minutes and standard deviation in this coefficient (in clear air).

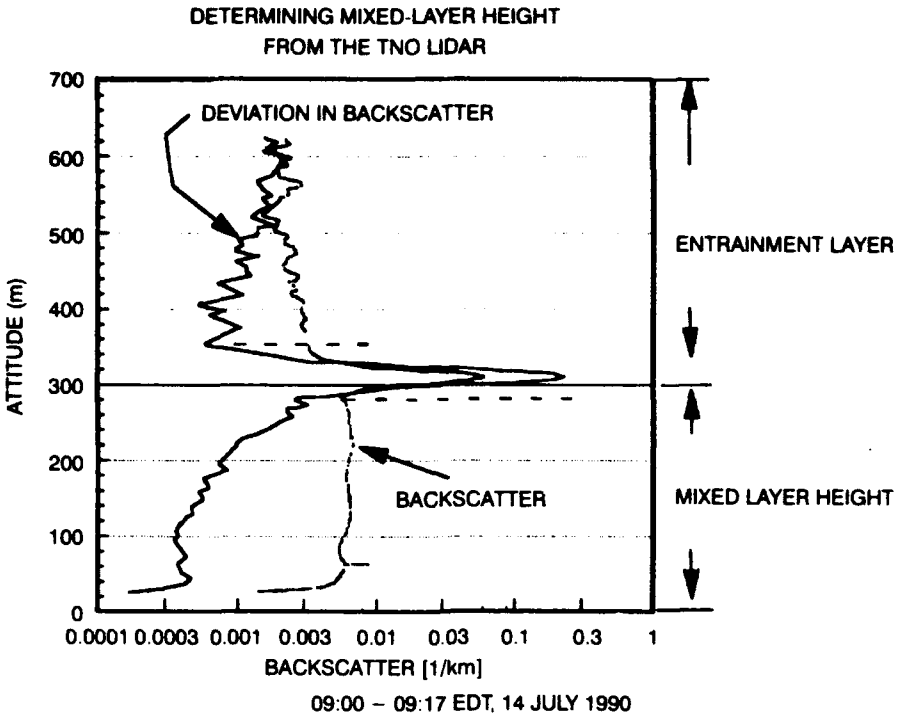

Figure 20. As in figure 19, but in the presence of clouds.

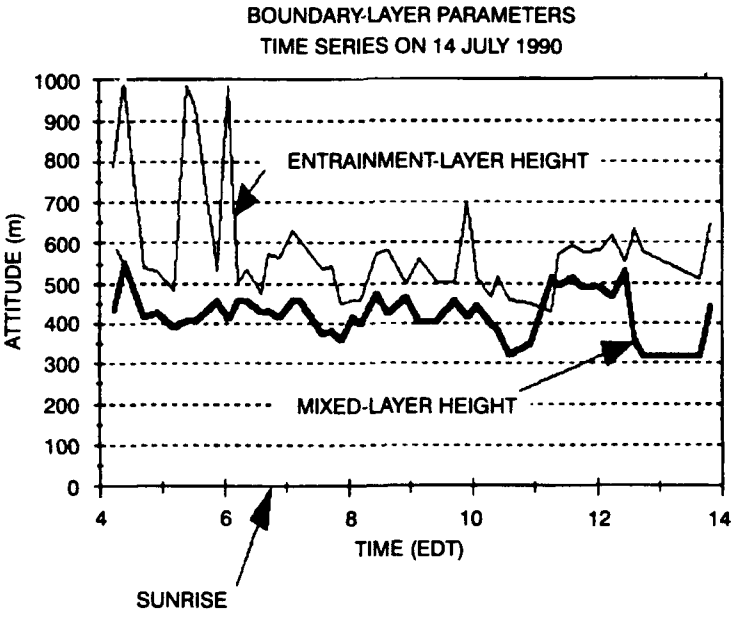

Figure 21. Mixed-layer height (thick line) and entrainment-layer height (thin line) from 04:00 to 14:00 on 14 July, as derived from TNO lidar.

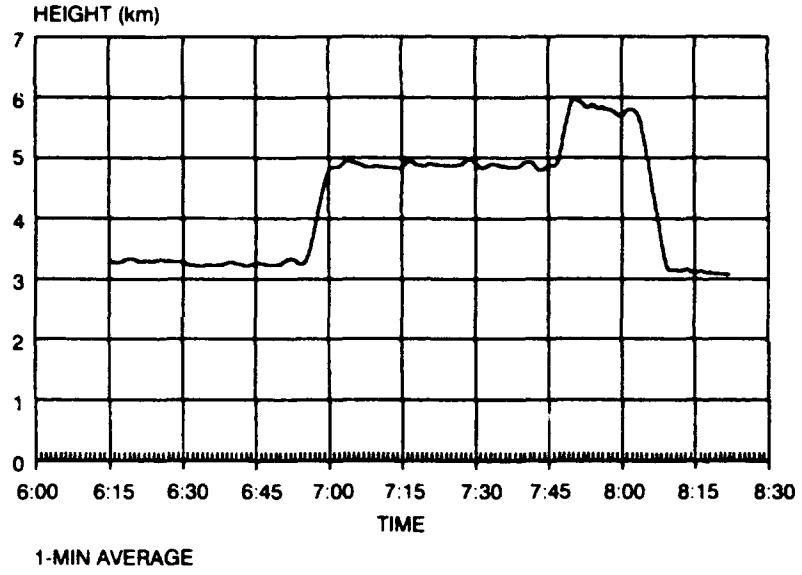

Figure 22. A segment of the time history of the aircraft altitude determined from the NRL lidar data for 14 July 1990.

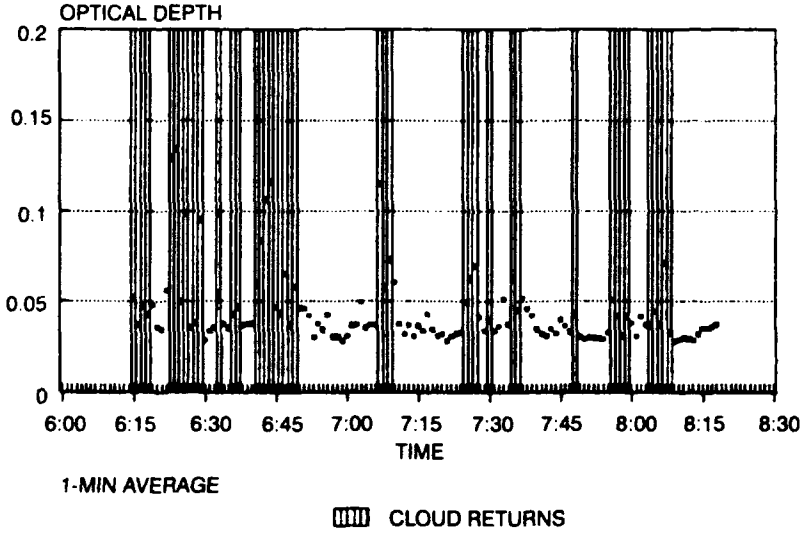

Figure 23. A time history of the optical depth between the NRL aircraft and the ocean surface on 14 July 1990. Note the time span here is the same as in figure 22. Shaded areas represent returns from clouds.

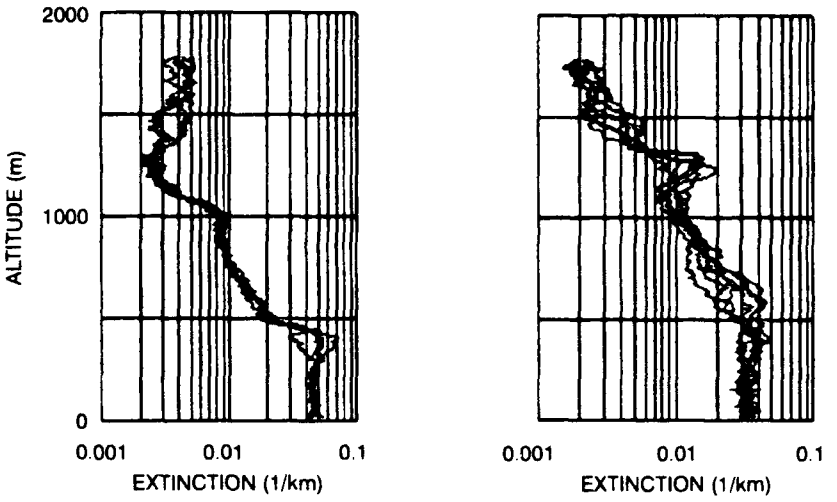

Figure 24. Extinction profiles obtained from NRL lidar returns showing the results of two sets of lidar shots taken at different times and places on 14 July 1990. The left-hand plot shows four shots taken between 06:38:56 and 06:39:04 at a position of 24.1°N, 80.58°W. The right-hand plot shows six shots taken a short time later at 24:38°N, 80.58°W.

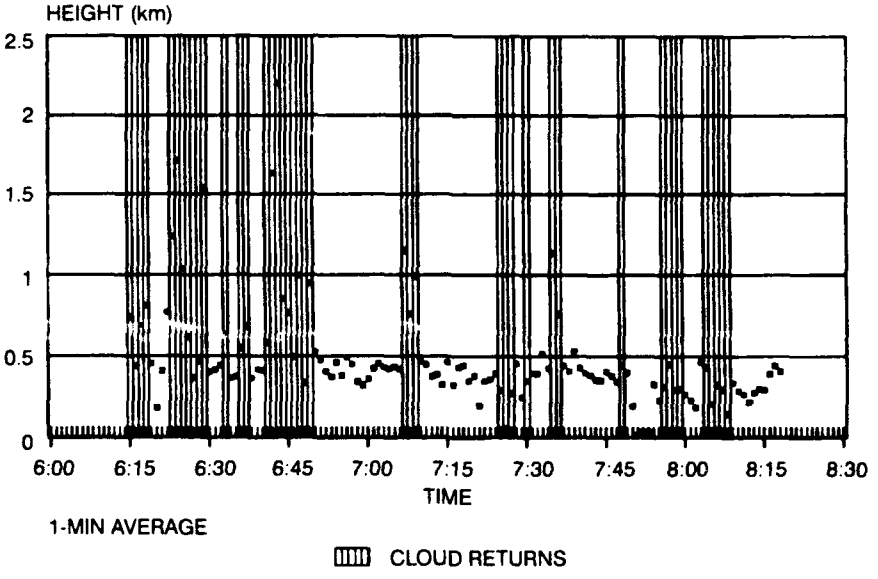

Figure 25. A time history of the boundary-layer height determined from major variations in the lidar-determined extinction profiles.

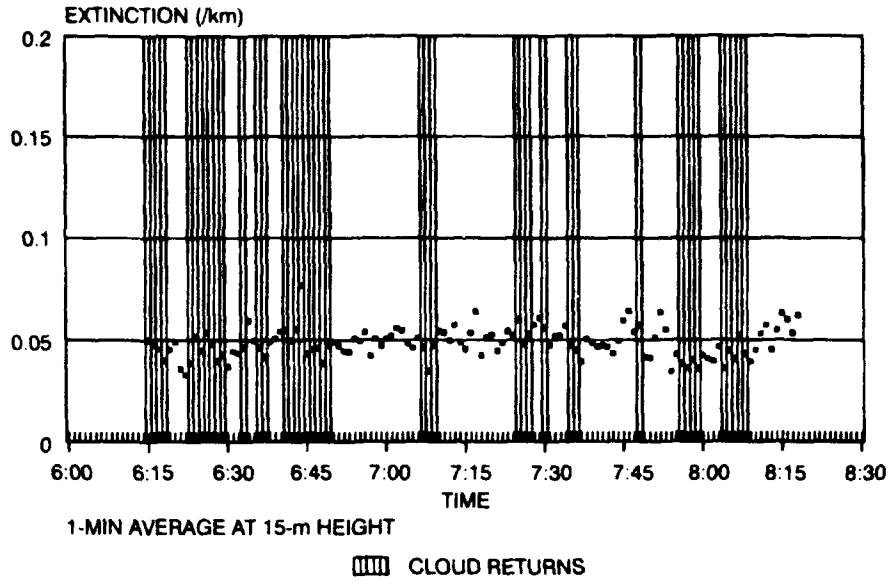

Figure 26. A time history of the surface (15 m) extinction as determined by the NRL downward-looking lidar (at 1.06 μ) on 14 July 1990 during KEY-90.

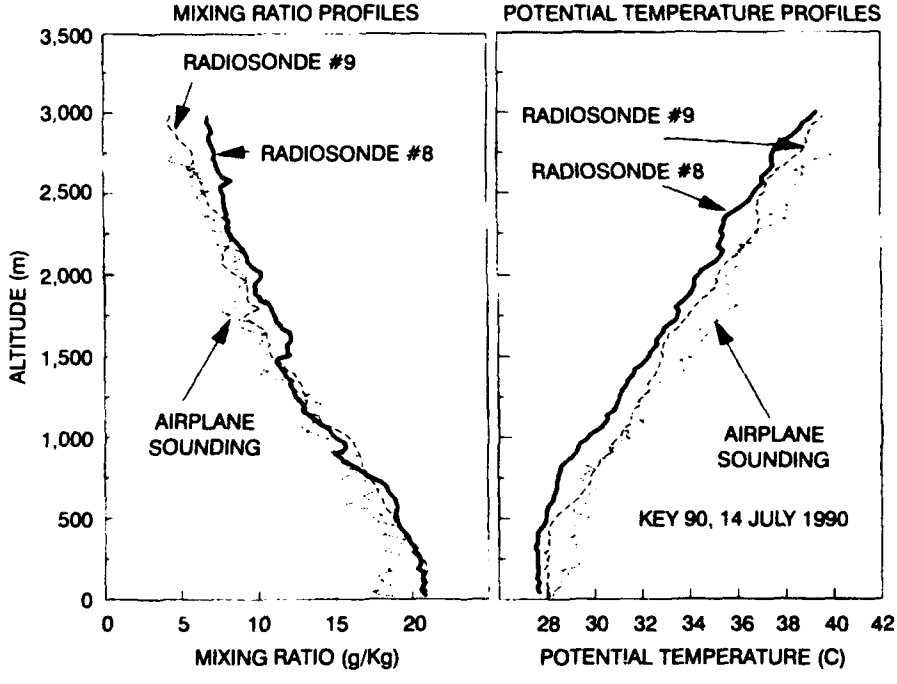

Figure 27. Meteorological profiles taken at the boat on 14 July 1990. Note that all three of the profiles show essentially the same general shape but that the offset of a degree or two in air temperature is probably due to both an offset in time, location, and different calibration factors. These differences do not make any appreciable difference in the performance of NOVAM in these cases.

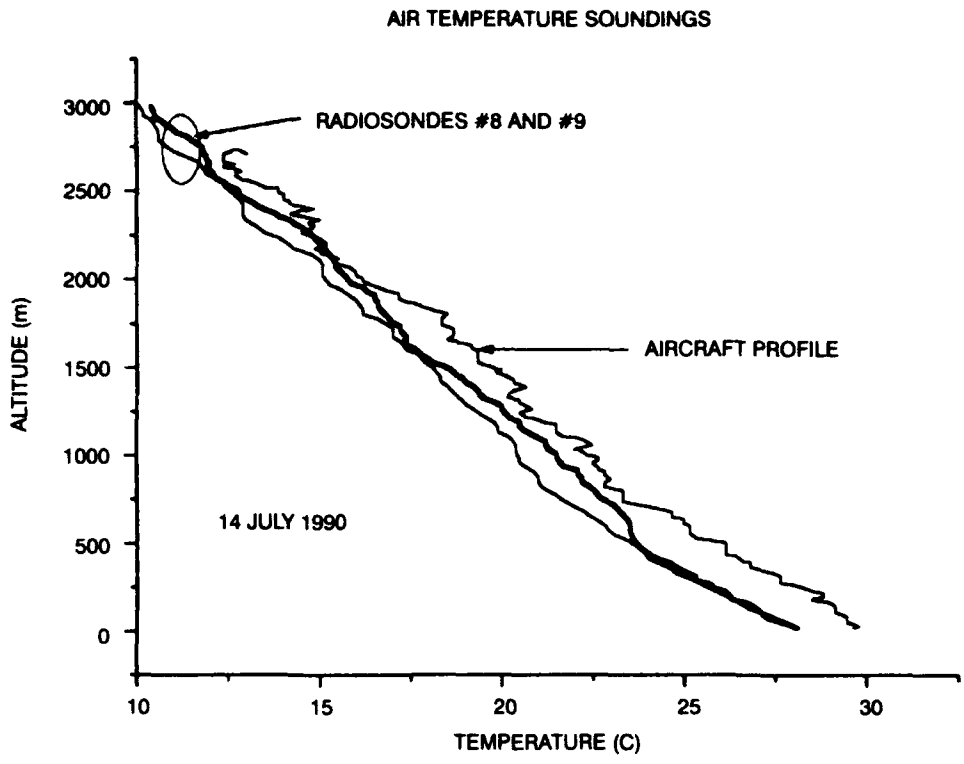

Figure 28. Temperature profiles plotted from the same three profiles shown in figure 27 from 14 July 1990. The hint of some sort of stable layer shown in figure 27 at 500 m is not at all evident in the temperature profile presentation. There are fluctuations and kinks in these curves, but the main temperature decreased monotonically as the altitude increased.

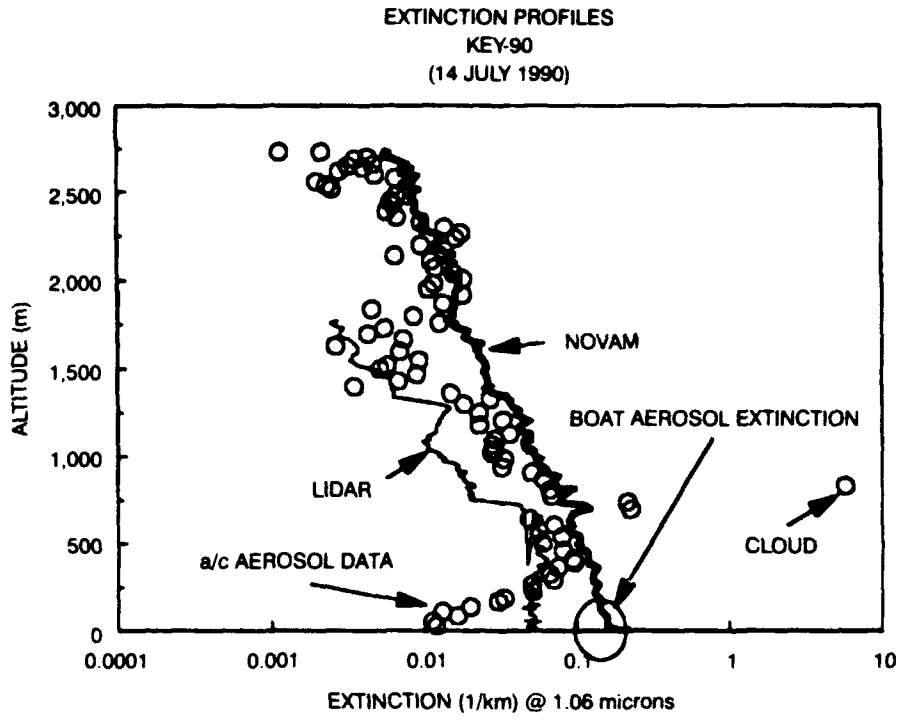

Figure 29. A composite plot of various types of extinction data taken during KEY-90 on 14 July 1990 for a wavelength of 1.06 μ. The small circles are the data calculated from the aircraft aerosol size distribution measurements. The large circle at the surface is the extinction calculation from an hour average of the boat aerosol size distribution measurement. The thin line is the NRL lidar extinction estimate at approximately the same time and place. Finally, the thick line is the NOVAM estimate of extinction at 1.06 μ for the particular set of surface and radiosonde data available at the site. Note that the aircraft inadvertently entered a cloud in the process of making its profile and a few large extinction values are noted in the data.

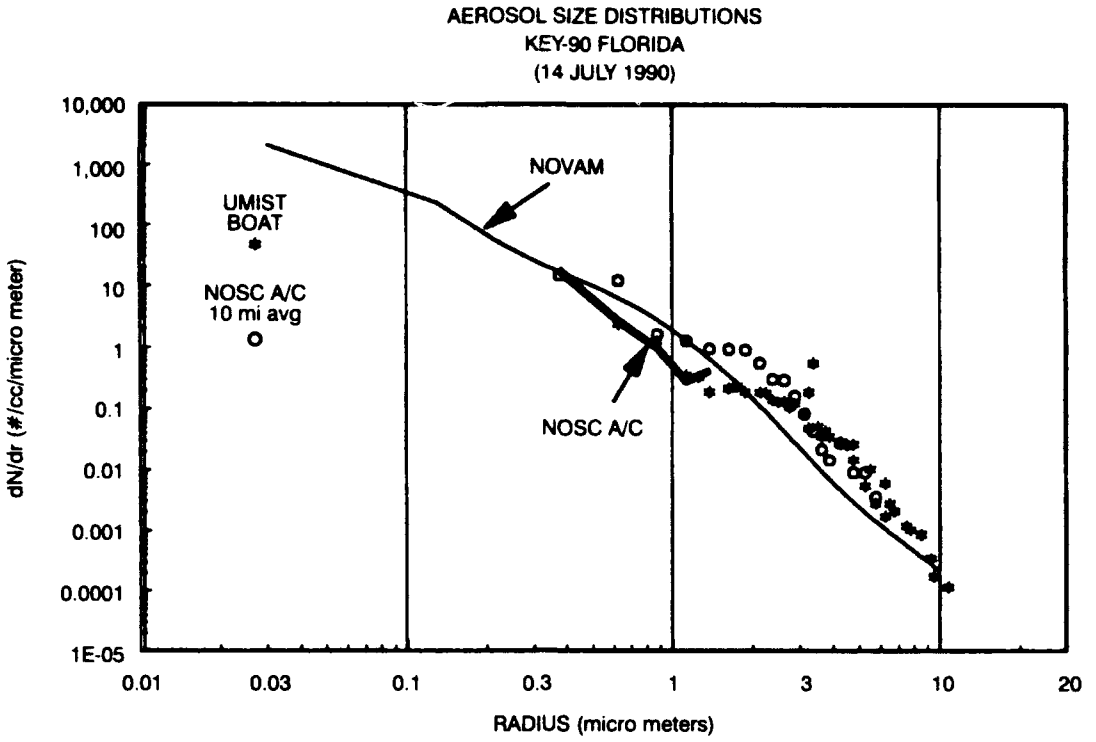

Figure 30. Aerosol size distributions on 14 July 1990 taken within 100 m of the sea. The stars are the dN/dr values taken from the boat instrumentation and are essentially long-term averages. The heavy solid line is data from the NOSC aircraft, but it was taken at the lowest layers of the profile, and thus the sampling time was somewhat limited and larger particles were not counted. However, when flying at a very low level for 10 miles over the sea, the average dN/dr values are shown by the circles and match those of the boat well. The solid thin line is that calculated from NOVAM at the surface and is based on the local meteorological data available.

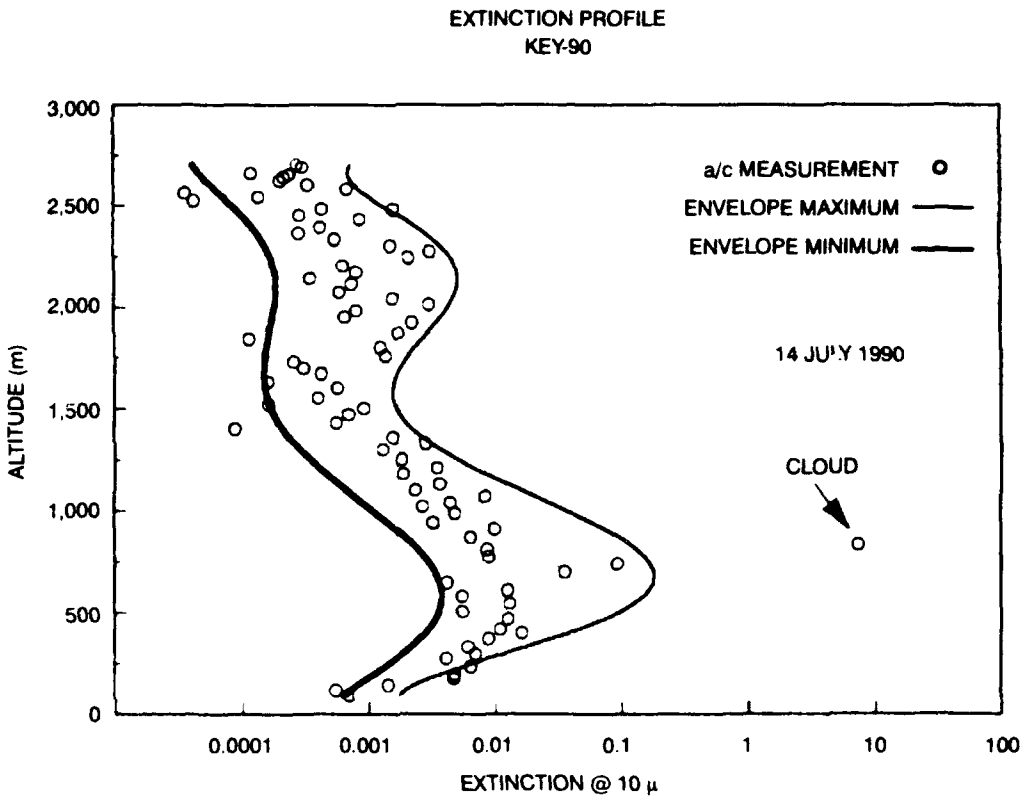

Figure 31. The extinction profile obtained from a/c aerosol measurements for a wavelength of 10 μm for 14 July 1990. An envelope determined from the data encloses the observed points. The method of determining this envelope is discussed in the text. The width of the envelope determines the uncertainty in the measured profile. The variations are either produced by homogeneous irregularities in the atmosphere or by inadequate statistical sampling of the aerosol data.

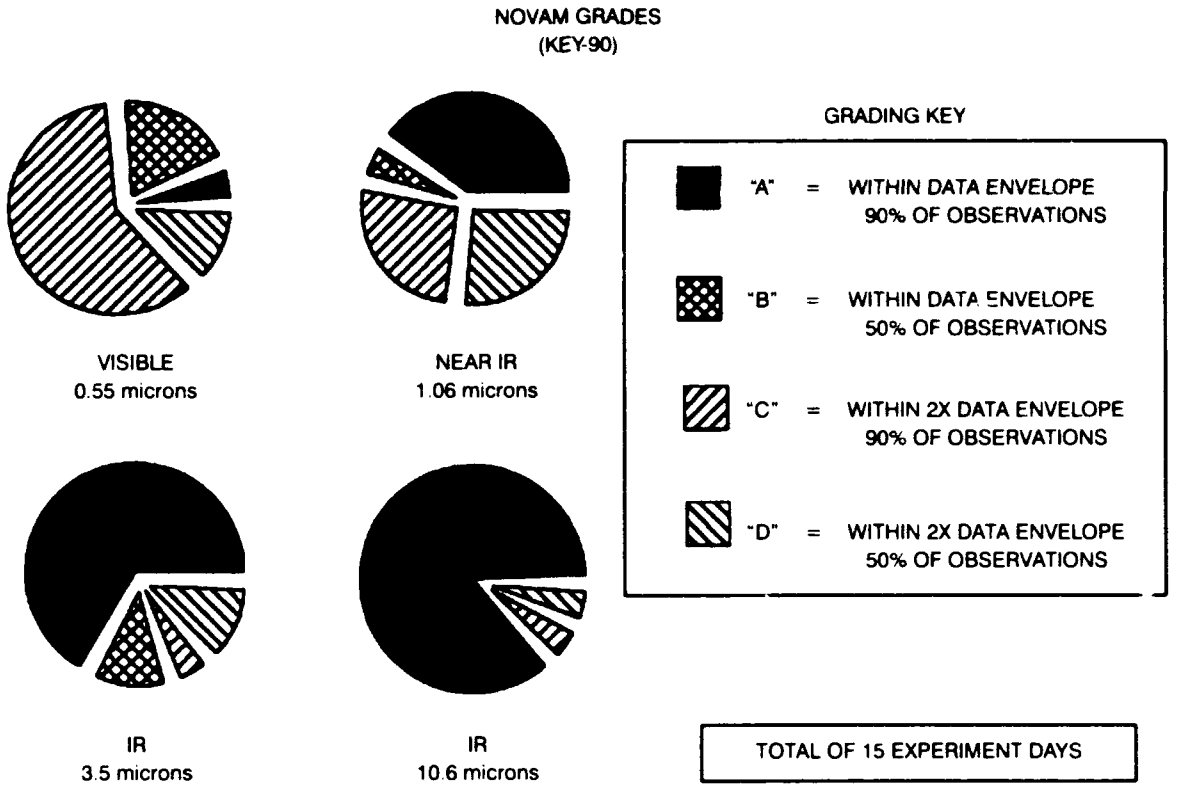

Figure 32. Grades for NOVAM performance during all the experiments from KEY-90. Grades are subjectively based and determined by the criterion shown in the grading key in the figure.

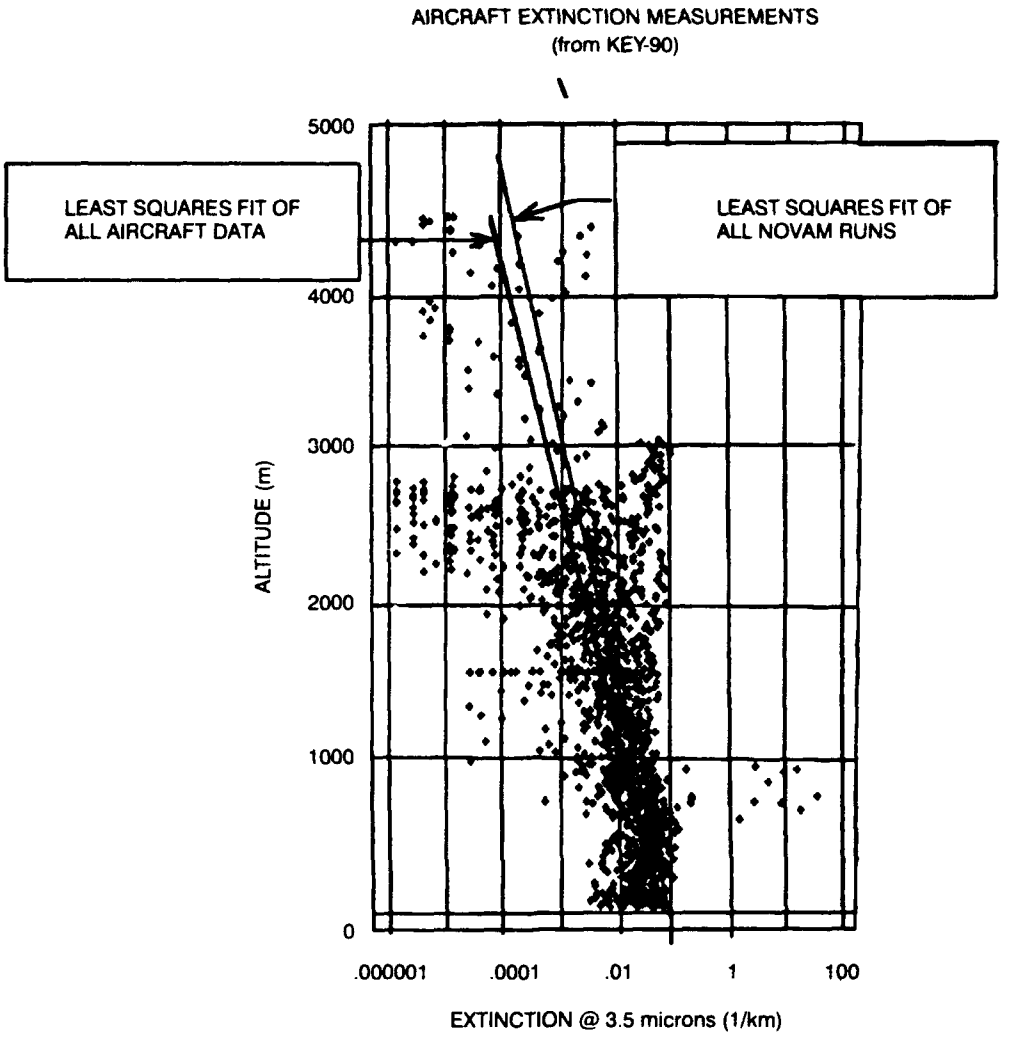

Figure 33. A combined plot of all KEY-90 3.5-μm extinction data obtained from a/c measurements of aerosol size distribution. These points are plotted together on the same chart and exhibit a mean characteristic. Least square fits to the data and also from all the NOVAM runs are plotted as lines in the figure.

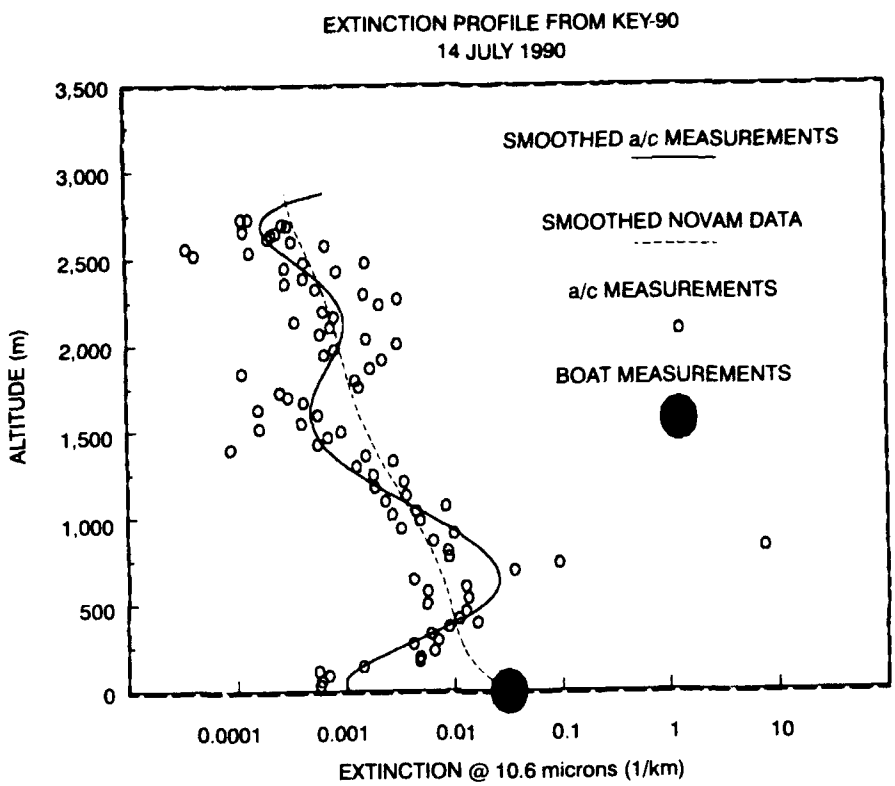

Figure 34. A profile plot of the 10.6-μ extinction on 14 July 1990 during KEY-90 in which individual observations of a/c extinction calculations are shown as open circles in the plot. A sixth-order smooth polynomial is fitted to the observed points and plotted as a solid line in the figure. A similarly smoothed curve from the NOVAM calculations is plotted as the dashed line in the figure. The boat extinction data calculated from the boat aerosol data are shown by the large black circle.

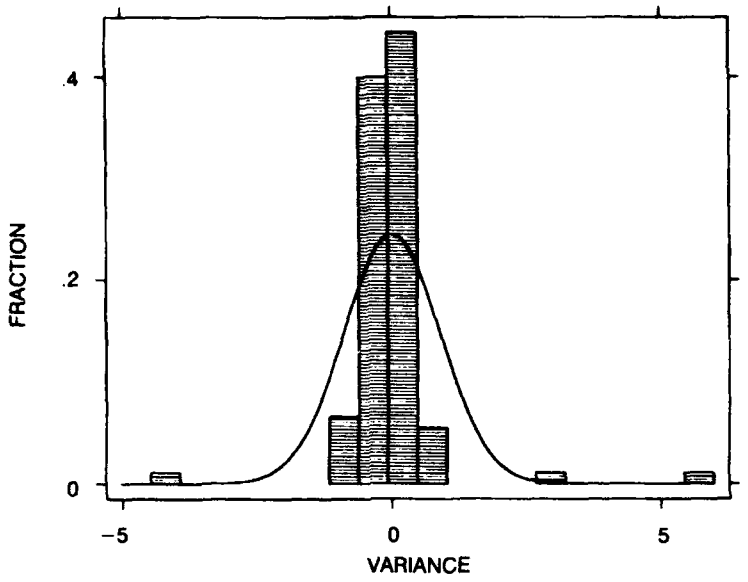

Figure 35. A plot of the histogram of the variance of the log of the aircraft extinction measurements at 10.6-μ taken from the log of the smooth "average" profile as determined by the regression fit on 14 July 1990 during KEY-90. The data show some observations considerably outside of the normal distribution.

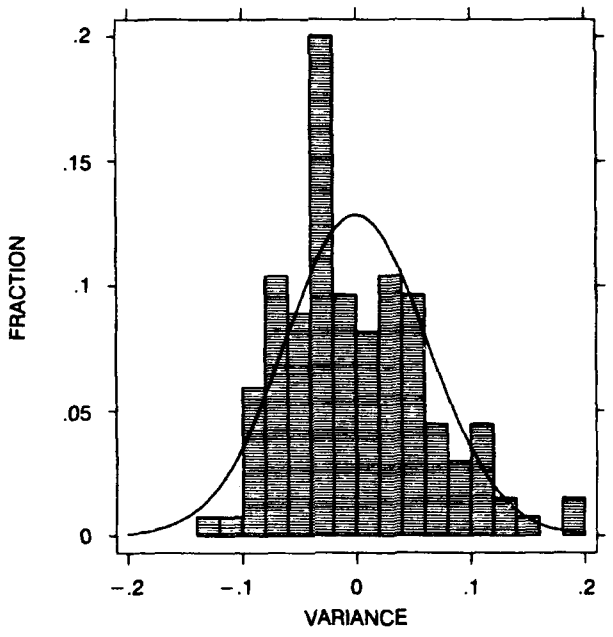

Figure 36. A plot of the same analysis done in figure 35, but this time, the variance is that of the NOVAM extinction data from the smooth "average" plot that we obtained from the regression analysis.

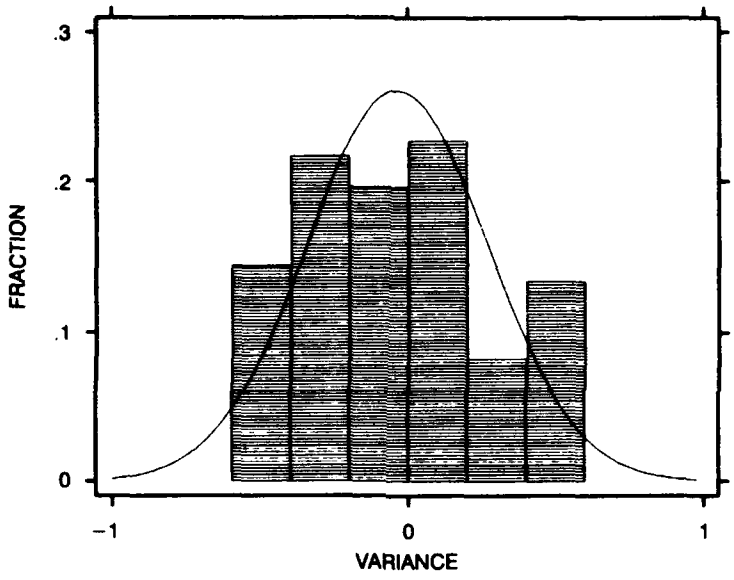

Figure 37. This is a plot of the variance between the log of the smoothed aircraft 10.6-μ extinction profile data and the log of the average NOVAM calculation for this case of 14 July 1990 during KEY-90. This is a method of the level-by-level variations, which can be considered as a form of noise, and to see how well NOVAM and the measurments agree in the best set of situations.

REPORT DOCUMENTATION PAGE

Form Approved
OMB No. 0704-0188

1 AGENCY USE ONLY *(Leave blank)*	2 REPORT DATE	3 REPORT TYPE AND DATES COVERED
	September 1993	Final

4 TITLE AND SUBTITLE
NOVAM EVALUATION UTILIZING ELECTRO-OPTICS AND METEOROLOGICAL DATA FROM KEY-90

5 FUNDING NUMBERS
PE: 0602435N
WU: DN302215

6 AUTHOR(S)
S. G. Gathman et al.

7 PERFORMING ORGANIZATION NAME(S) AND ADDRESS(ES)
Naval Command, Control and Ocean Surveillance Center (NCCOSC)
RDT&E Division
San Diego, CA 92152-5001

8 PERFORMING ORGANIZATION REPORT NUMBER
TR 1608

9 SPONSORING/MONITORING AGENCY NAME(S) AND ADDRESS(ES)
Naval Research Laboratory Detachment
Stennis Space Center
Mississippi 34529-5000

10 SPONSORING/MONITORING AGENCY REPORT NUMBER

11 SUPPLEMENTARY NOTES

12a DISTRIBUTION/AVAILABILITY STATEMENT
Approved for public release; distribution is unlimited.

12b DISTRIBUTION CODE

13 ABSTRACT *(Maximum 200 words)*

An experiment known as KEY-90 took place in the Straits of Florida, from 2 to 19 July 1990. The center of operations was the town of Marathon, which is in the center of the Florida Keys. The experiment's principal objective was to verify the Naval Oceanic Vertical Aerosol Model (NOVAM) and its kernel, the Navy Aerosol Model (NAM), in a tropical ocean scenario. The data collected during KEY-90 included aerosol particle-size distributions, lidar profiles, pertinent meteorological observations, and ocean surface parameters. Shore stations, a boat, buoys, radiosondes, and aircraft provided platforms to obtain these data. These measurements determined the structure of the atmospheric surface boundary layer. This report presents a general overview of these experiments, a description of the data available from KEY-90, and specific examples of these data for 14 July 1990.

14 SUBJECT TERMS
Naval Aerosol Model
lidar profiles
meteorological observations
ocean surface parameters

15 NUMBER OF PAGES
75

16 PRICE CODE

17 SECURITY CLASSIFICATION OF REPORT	18 SECURITY CLASSIFICATION OF THIS PAGE	19 SECURITY CLASSIFICATION OF ABSTRACT	20 LIMITATION OF ABSTRACT
UNCLASSIFIED	UNCLASSIFIED	UNCLASSIFIED	SAME AS REPORT

21a. NAME OF RESPONSIBLE INDIVIDUAL	21b. TELEPHONE *(Include Area Code)*	21c. OFFICE SYMBOL
S. G. Gathman	(619) 553-1418	Code 543

INITIAL DISTRIBUTION

Code 0012	Patent Counsel	(1)
Code 02712	Archive/Stock	(6)
Code 0274B	Library	(2)
Code 50	H. O. Porter	(1)
Code 54	J. H. Richter	(1)
Code 543	R. A. Paulus	(1)
Code 543	D. R. Jensen	(1)
Code 543	K. M. Littfin	(1)
Code 543	C. R. Zeisse	(1)
Code 543	C. P. McGrath	(1)
Code 543	S. G. Gathman	(100)

Defense Technical Information Center
Alexandria, VA 22304–6145 (4)

NCCOSC Washington Liaison Office
Washington, DC 20363–5100

Center for Naval Analyses
Alexandria, VA 22302–0268

Navy Acquisition, Research and Development
Information Center (NARDIC)
Washington, DC 20360–5000

GIDEP Operations Center
Corona, CA 91718–8000

NCCOSC Division Detachment
Warminster, PA 18974–5000

Naval Research Laboratory
Washington, DC 20375–5000 (10)

Naval Postgraduate School
Monterey, CA 93943–5100 (10)

Gerber Scientific, Inc.
Reston, VA 22090 (2)